EFFICIENCY CALIBRATION OF NaI DETECTORS FOR A MEASUREMENT OF THE $^{12}C(n, 2n)^{11}C$ CROSS SECTION

By

Thomas James Eckert

A thesis submitted in partial fulfillment of the
requirements for the degree of

Bachelor of Science

Houghton College

June 14, 2016

Signature of Author……..……..
Department of Physics
June 14, 2016

……..
Dr. Mark Yuly
Professor of Physics
Research Supervisor

……..
Dr. Brandon Hoffman
Associate Professor of Physics

EFFICIENCY CALIBRATION OF NaI DETECTORS FOR A MEASUREMENT OF THE $^{12}C(n, 2n)^{11}C$ CROSS SECTION

By

Thomas James Eckert

Submitted to the Department of Physics
on June 14, 2016 in partial fulfillment of the
requirement for the degree of
Bachelor of Science

Abstract

One possible inertial confinement fusion diagnostic involves tertiary neutron activation of a carbon disk via the $^{12}C(n, 2n)^{11}C$ reaction. A recent experiment to measure this reaction cross section involved coincidence counting the annihilation gamma rays produced by the positron decay of ^{11}C. This requires an accurate value for the full-peak coincidence efficiency of the NaI detector system. The GEANT 4 toolkit was used to develop a Monte-Carlo simulation of the detector system, which was used to calculate the required efficiencies. For validation, simulation predictions have been compared with the results of two types of experiments. In the first, full-peak coincidence positron annihilation efficiencies were measured for ^{22}Na decay positrons that annihilate in a small plastic scintillator. In the second, a NIST-calibrated ^{68}Ge source was used. A comparison of calculated with measured efficiencies, and the resulting $^{12}C(n, 2n)^{11}C$ cross sections, are presented.

Thesis Supervisor: Dr. Mark Yuly
Title: Professor of Physics

This material is based upon work supported by the Department of Energy [National Nuclear Security Administration] University of Rochester "National Inertial Confinement Program" under Award Number(s) DE-NA0004144.

TABLE OF CONTENTS

TABLE OF FIGURES AND TABLES

Chapter 1

MOTIVATION FOR EFFICIENCY MEASUREMENT

The areal density of Inertial Confinement Fusion (ICF) can be measured using the $^{12}C(n, 2n)^{11}C$ reaction. In this diagnostic, a graphite disk is exposed to high-energy neutrons from ICF. The disk is then placed between detectors that measure the fraction of graphite in the disk that underwent the reaction by detecting gamma rays in coincidence, which gives the areal density.

1.1 The $^{12}C(n, 2n)^{11}C$ Reaction as a Diagnostic for Fusion

When nuclei lighter than iron undergo a fusion reaction, a fraction of their binding energy is released. Ignition of the fusion fuel is achieved when the energy released into the fuel by the reaction creates high enough temperatures to make fusion self-sustaining. ICF above this ignition threshold has a net-positive energy output and can be operated as a source for a power plant. Proximity to ignition is correlated to the areal density of ICF, which can be measured using the $^{12}C(n, 2n)^{11}C$ reaction.

1.1.1 Inertial Confinement Fusion

ICF uses pulsed lasers to ablate a thin spherical shell, usually composed of plastic, containing a mixture of deuterium and tritium. The ablation of the shell forces the fuel inwards. The implosion of nuclear fuel produces a core temperature of 10^8 K [1]. This is an order of magnitude hotter than the core of the Sun. These temperatures are necessary to increase the likelihood of fusion reactions. Heat loss from the fuel makes reaching ignition difficult. The period of time within which the temperature and density are high enough to reach ignition is on the order of nanoseconds [1].

The fuel inside the plastic shell is composed of deuterium (D) and tritium (T). At the high temperatures achieved, the fuel becomes plasma. In this state, deuterium and tritium become ionized, leaving the bare nuclei, deuterons and tritons respectively.

The DT nuclear reaction releases more energy than D+D or T+T, but all three can occur during ICF. The nuclear fusion of deuterons with tritons produces an alpha particle, α, and a neutron, n, which carries 80% of the energy from the reaction,

$$\mathrm{D} + \mathrm{T} \rightarrow \alpha(3.5\ \mathrm{MeV}) + \mathrm{n}(14.1\ \mathrm{MeV}). \quad (1)$$

The neutron, which usually escapes outside the implosion, will travel further before reacting than the charged alpha particle, which quickly loses its energy into the fuel due to its charge, heating the fuel in the process [2]. Rather than escaping, a neutron can sometimes scatter from tritons or deuterons.

1.1.2 Ignition and Areal Density

ICF can only produce a net positive output of energy if the fuel reaches ignition, a state where external energy input is no longer needed to heat the fuel. It is hoped that this can be achieved by finding the correct parameters to maintain the needed areal density and temperature of the fuel in order to increase the rate of fusion reactions.

This rate is determined by two values: the cross section of the fusion reaction and the areal density of the fuel. The cross section of fusion, which is proportional to the probability of the reaction, depends on the energy, or temperature, of the fuel. Areal density is determined by hydrodynamic variations within the plasma. It is the product of the radius and density of the core and difficult to calculate or measure using current methods.

A technique has been developed for measuring the areal density of the ICF core as well as the hydrodynamic stability of the implosion. The number of neutrons produced by the fusion reaction is a function of the areal density of the compressed core. Graphite disks placed in the ignition chamber can only be activated via the $^{12}C(n, 2n)^{11}C$ reaction by incident neutrons with energies above 20.296 MeV [3]. Tertiary neutrons are the only neutrons produced by the ICF fusion reaction with energies above this threshold, and can be used to measure the areal density.

1.1.3 Tertiary Neutrons

Figure 1 is a plot of the predicted yield of neutrons from ICF at the National Ignition Facility (NIF) as a function of their energy. Tertiary neutrons are the most energetic neutrons typically produced by DT ICF reactions. They are the result of fusion of knock-on ions in the fuel, that is, ions from which neutrons have previously scattered.

The reaction in Equation 1 produces primary neutrons with kinetic energy of 14.1 MeV. These neutrons can elastically scatter from deuterons and tritons in the fuel:

$$\mathrm{n\ (14.1\ MeV) + D \rightarrow n' + D'(0 - 12.5\ MeV)} \tag{2}$$

and

$$\mathrm{n\ (14.1\ MeV) + T \rightarrow n' + T'(0 - 10.6\ MeV)} \tag{3}$$

where n' is a secondary neutron – so called because it is the result of elastic scattering of primary neutrons. The products D' and T' are "knock-on" ions. This reaction will, in most cases, increase the kinetic energy of the D and T reactants. Any subsequent fusion reactions involving these ions will produce more energetic products than primary fusion.

The "knock-on" ions that undergo fusion reactions can produce tertiary neutrons, n", by

$$\mathrm{D'\ (0 - 12.5\ MeV) + T \rightarrow \alpha + n"\ (12.0 - 30.1\ MeV)} \tag{4}$$

or

$$\mathrm{T'\ (0 - 10.6\ MeV) + D \rightarrow \alpha + n"\ (9.2 - 28.2\ MeV).} \tag{5}$$

Tertiary neutrons are so called because they are produced by the tertiary reaction, two degrees separated from the primary fusion reaction. They are the only neutrons produced in significant numbers that have energies above the threshold required for the $^{12}C(n, 2n)^{11}C$ reaction. Because of this, they can activate

the carbon without the primary, secondary, or down-scattered neutrons from the reaction having any effect.

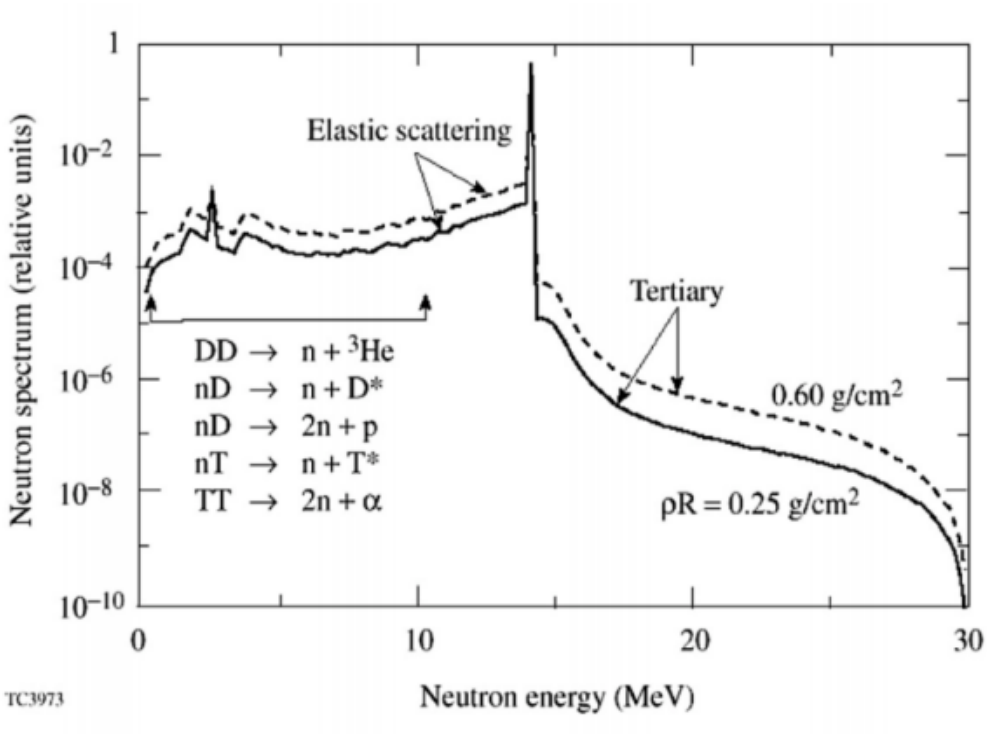

Figure 1. The predicted number of neutrons produced by ICF reactions at the National Ignition Facility plotted as a function of their energies. Calculations of neutron energies were made for two values of areal density. Tertiary neutrons have the highest energies in the DT fusion reaction. Figure taken from Ref [2].

The yield of tertiary neutrons is approximately proportional to $(\rho R)^2$ for values of areal density less than 0.1 g/cm^2, such as occur at the Laboratory for Laser Energetics (LLE) in Rochester, NY. For areal densities above 0.1 g/cm^2 - such as occur at the National Ignition Facility (NIF) in Livermore, CA - the yield of n" is proportional to ρR [2]. When multiple carbon disks are placed around the fuel, they can be used to map the hydrodynamic isotropy of the fusion plasma [4].

1.1.4 Measuring the $^{12}C(n, 2n)^{11}C$ Cross Section

Before areal density can be measured using this method, a more accurate measurement of the cross section for the $^{12}C(n, 2n)^{11}C$ reaction must be made. Published values [6-12] for this cross section currently disagree with each other by up to a factor of two in the 20-30 MeV region of interest, as shown in Figure 2. The methods used to calculate these cross sections are covered in detail in Ref [5].

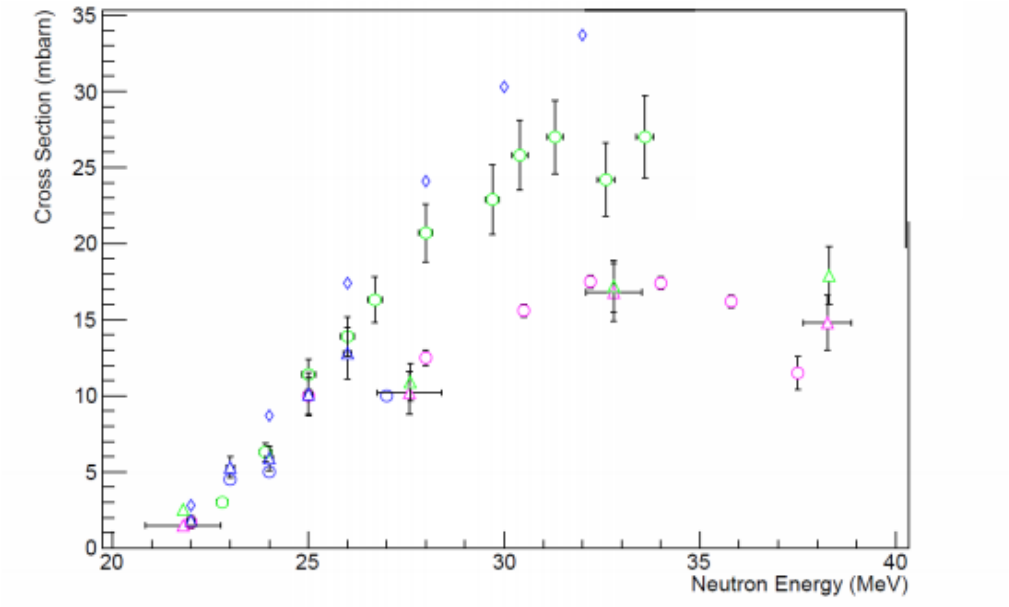

Figure 2. Published cross-sections for the $^{12}C(n, 2n)^{11}C$ reaction from Brolley et al. [6] (blue circles), Brill et al. [7] (pink circles), Anders et al. [8] (green circles), Welch et al. [9] (blue triangles), Soewarsono et al. [10] (pink triangles), Uno et al. [11] (green triangles), and Dimbylow [12] (blue diamonds). These measurements disagree by up to a factor of two in the region of interest from 20 to 30 MeV.

An experiment, shown in Figure 3, to measure the cross section with an uncertainty of less than 5% was carried out at Ohio University in the summers of 2012 and 2013 by a collaboration of scientists and students from SUNY Geneseo, Houghton College, the Laboratory for Laser Energetics, and Ohio University [5]. The Ohio University pelletron accelerator shot a deuteron beam with energies up to 9.2 MeV at a tritium tritide target. The DT reaction was used to produce monoenergetic neutrons for

numerous energy settings above 20 MeV. The neutrons caused ^{12}C in the polyethylene disk, carbon shields, and carbon disk to undergo the $^{12}C(n, 2n)^{11}C$ reaction.

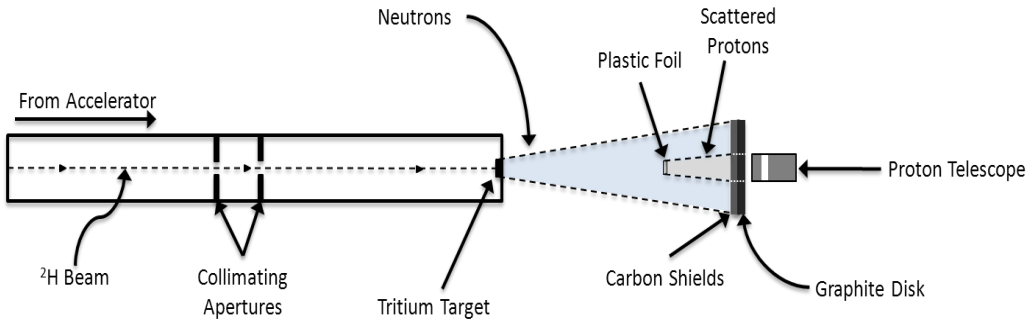

Figure 3. Experiment setup at Ohio University. The Ohio University pelletron accelerator shot a collimated beam of deuterons at a tritium target. This emitted monoenergetic neutrons with energies high enough to initiate the $^{12}C(n, 2n)^{11}C$ reaction in a graphite disk and plastic foil. The neutron flux was calculated by measuring the protons scattered by neutrons and using the H(n, p) reaction cross section.

Neutrons with energies above 20.236 MeV [3] that are incident on ^{12}C can interact with a carbon nucleus and remove a neutron via the $^{12}C(n, 2n)^{11}C$ reaction

$$^{12}C + n \rightarrow {}^{11}C + n + n\,. \tag{6}$$

The ^{11}C produced by the reaction is unstable. It will β^+-decay into ^{11}B with a half-life of 20.334 minutes [13]. This decay releases a positron, e^+, and a neutrino, ν.

$$^{11}C \rightarrow {}^{11}B + e^+ + \nu\,. \tag{7}$$

The positron annihilates with an atomic electron in the surrounding material. This annihilation produces two 511 keV back-to-back gamma rays. The emission of gamma rays at this energy and with this alignment is a unique signature of ^{11}C decay that can be isolated from background radiation. Two detectors placed on either side of the decaying graphite can detect the back-to-back 511 keV gamma rays simultaneously, confirming a ^{11}C decay event.

After irradiation, the disks and shields were each removed from the target stand and taken to an isolated counting room, where they were placed flush between pairs of NaI detectors as shown in Figure 4. The ^{11}C decays were counted by using the back-to-back gamma coincidences produced by positron annihilation. The detectors counted coincidence 511 keV gamma rays using a multi-parameter system. Gamma rays that entered the detectors within about 300 ns of each other were considered to have been emitted from the same beta-decay event. This technique allowed growth curves of ^{11}B in the carbon to be measured.

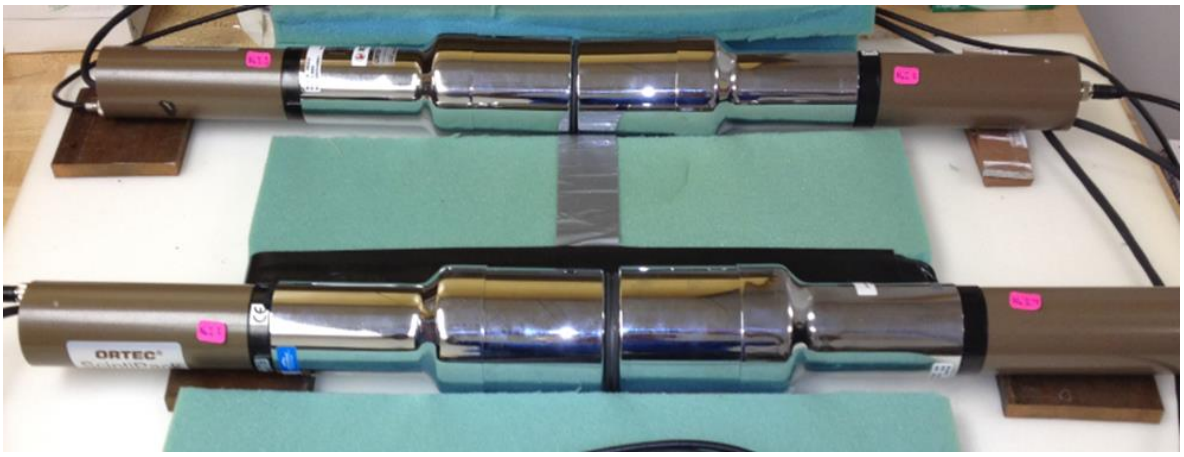

Figure 4. Counting station at the Ohio University Experiment in 2013. This setup was used to measure ^{11}C beta-decay in the carbon and polyethylene disks by detecting, in coincidence, 511 keV gamma rays released by positron annihilation.

To complete the measurement of the cross section, the neutron flux of the beam from the accelerator in Figure 3 was measured. Some of the neutrons from the accelerator incident on the polyethylene (CH_2) disk were elastically scattered by the hydrogen nuclei, emitting protons by the $^1H(n, p)$ reaction [14, 15]. These protons could pass through a 2.54 cm diameter hole in the center of the graphite disk. Carbon shields with a cumulative thickness of 3.85 mm were placed on the upstream face of the graphite disk around this hole. This protected the 8.9 mm thick graphite disk from incident protons scattered from the plastic. The proton flux was measured using a dE-E proton-telescope behind the hole in the graphite disk. This allowed the neutron flux to be determined using the $^1H(n, p)$ cross section, which is well-

measured. The neutron flux and ^{11}B growth curves were used to determine the $^{12}C(n, 2n)^{11}C$ cross section at each incident neutron energy.

1.2 Scintillation Detectors

Counting the number of ^{11}C that underwent the $^{12}C(n, 2n)^{11}C$ reaction is vital to measuring the cross section of the reaction. However, scintillation detectors, such as the NaI detectors shown in Figure 4 that were used for this experiment cannot measure 100% of the gamma rays emitted from a source. Gamma rays will deposit energy into solid substances they pass through. Materials that exhibit fluorescent properties can absorb this energy and emit flashes of light called scintillations. This is how the NaI scintillation detectors used in this experiment worked.

1.2.1 Physical Limitations of Detector Efficiency

Scintillation detectors are incapable of detecting all of the gamma rays emitted by a radioactive source due to several limitations. The first involves the geometry of the detectors. If the source of radiation is not fully enveloped by the detectors - that is, it does not cover all 4π of the solid angle - then some fraction of the rays emitted by the source will not enter the detectors. The second limitation is the absorption coefficient of the scintillation material used to detect the gamma rays from the source. The likelihood of a gamma ray interacting to create a possible scintillation event in a detector is

$$S(E) = 1 - e^{-\mu(E)\Delta}, \tag{8}$$

where E is the energy of the photon, $\mu(E)$ is the absorption coefficient intrinsic to the material of the scintillation detector and dependent on the energy of the gamma ray, and Δ is the distance the ray travels through the detector. As neither the absorption coefficient nor the distance the gamma ray traveled can be infinite, S will never be 1. Thus, the percent of gamma rays that interact in the detector will never be 100%, even for a detector that fully encapsulates a source.

The third limitation is that gamma rays that interact may do so in such a way as to not be detected. For example, it is possible to have Compton scattering followed by escape of the gamma ray, which is not

counted because the energy deposited is too low. Fourth, photons from the scintillation could be absorbed in the detector or light guide before reaching the PMT.

1.2.2 Measuring Detector Efficiency

Although the detectors cannot measure all gamma rays produced by a source, the fraction of total gamma rays measured by a detector can be determined as its efficiency. It is important to know the efficiency so the number of gamma rays emitted by a source can be found from the number of gamma rays detected. To know the total number of gamma rays emitted by a source, one either must know the activity of the source or use a detector close to the source that can be triggered on an associated particle in coincidence with the scintillation detector system. Although the efficiency of the associated particle detector is not 100%, it will still allow for a sufficient measurement of the scintillation detector efficiency. Once the efficiency is known, dividing the number of gamma rays measured in an experiment by it, calibrates the measurement to produce the number of gamma rays emitted by the source.

The absolute efficiency, ε(abs), depends upon the solid angle of the detector. It is the ratio of gamma rays detected to the number emitted by a source,

$$\varepsilon(\text{abs}) = \frac{\text{gamma rays detected}}{\text{gamma rays emitted}} \,. \tag{9}$$

The intrinsic efficiency, ε(intr), does not depend on the solid angle of the detector. It is the ratio of gamma rays detected to the number that entered the detector,

$$\varepsilon(\text{intr}) = \frac{\text{gamma rays detected}}{\text{gamma rays in detector}} \,. \tag{10}$$

1.2.3 Total and Full-Peak Efficiencies

A scintillation detector can be used to produce a spectrum where the number of gamma rays detected in a given energy range is plotted as a function of their energy. The energy spectrum in Figure 5 was produced by a NaI scintillation detector measuring ^{22}Na using a multi-channel analyzer (MCA). The MCA plotted the number of gamma rays as a function of channels that correspond to the energy deposited by the gamma rays in the detector.

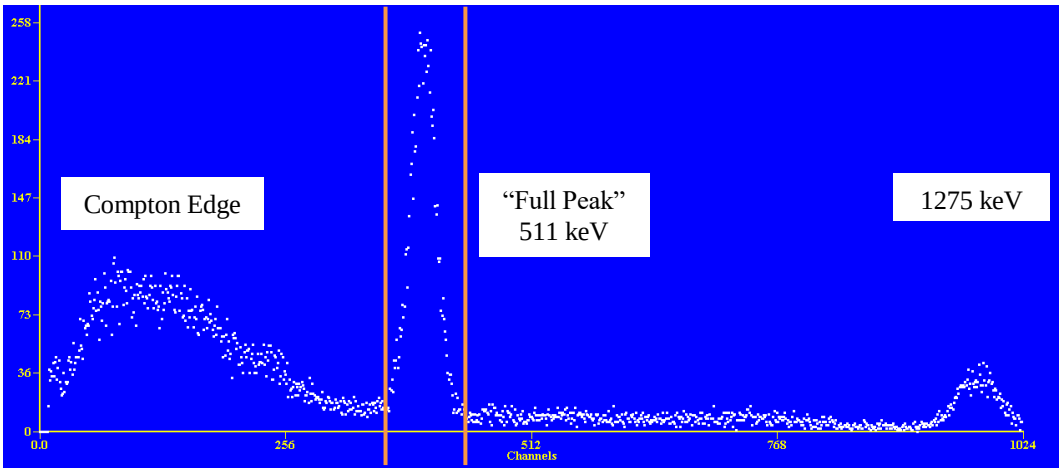

Figure 5. Energy spectrum from scintillator detector produced using a multi-channel analyzer. The number of gamma rays is plotted as a function of channels that correspond to their energies.

The spectrum in the figure has a wide peak between channels 0 and 250, which corresponds to gamma rays that Compton scattered in the detector. This is referred to as the Compton Edge. The peak between channels 300 and 500 corresponds to 511 keV gamma rays measured by the detector. The peak between channels 900 and 1024 was produced by 1275 keV de-excitation gamma rays emitted by the ^{22}Na source.

The ratio of all gamma rays measured in the spectrum to the number produced by a source was the total efficiency

$$\varepsilon(\text{tot}) = \frac{\text{"total" gamma rays detected}}{\text{gamma rays emitted}} . \tag{11}$$

The 511 keV peak was referred to as the "full-peak". Orange lines on either side of the peak show the range of channels, which were summed over. The ratio of gamma rays measured in the "full-peak" to the total number of gamma rays produced by a source was the full-peak efficiency

$$\varepsilon(\text{fp}) = \frac{\text{"full-peak" gamma rays detected}}{\text{gamma rays emitted}} . \tag{12}$$

1.2.4 Singles and Coincidence Efficiencies

The ^{11}C in the Ohio University Experiment were measured by counting positrons emitted from the beta-decay of ^{11}C into ^{11}B. These positrons paired off with atomic electrons and annihilated. In the center of mass frame of the positron-electron pair, momentum is zero and energy is roughly 1022 keV. To conserve energy and momentum, two 511 keV gamma rays are emitted from the annihilation 180-degrees from each other as shown in Figure 6.

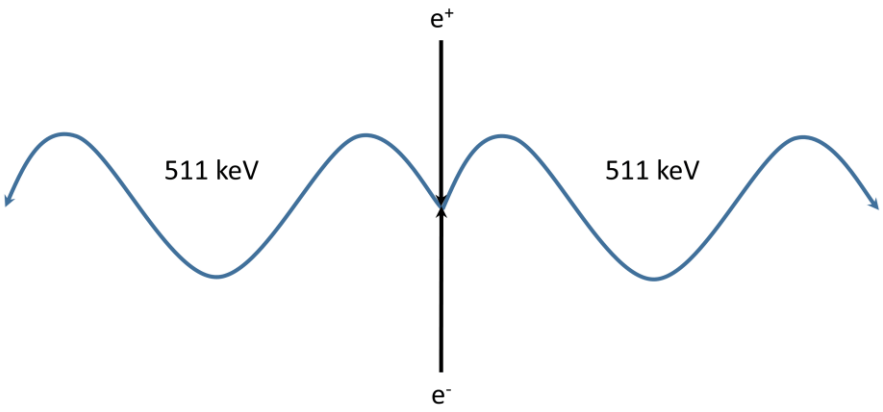

Figure 6. Positron-electron pairs annihilate and produce back-to-back 511 keV gamma rays to conserve energy and momentum.

A pair of NaI detectors measuring both 511 keV gamma rays at the same time could confirm a positron annihilation event and determine the number of ^{11}C in the graphite disks as in Figure 4. The fraction of

gamma rays pairs measured by each detector individually for this set up was the singles efficiency. The fraction of gamma rays measured by both detectors at the same time was the coincidence efficiency. Both types of efficiency were used to measure the $^{12}C(n, 2n)^{11}C$ cross section.

Chapter 2

2.1 Cross Section

The cross section for the $^{12}C(n, 2n)^{11}C$ reaction can be extracted from the ^{11}B growth curve and the proton flux using

$$\sigma = \frac{N_{11C}}{T_C} \frac{\lambda}{1\text{-}e^{-\lambda t}} \left(\frac{N_p}{N_n}\right) \frac{1}{N_p}. \tag{13}$$

where σ is the cross section, N_{11C} is the number of ^{11}C in the target that has been determined by fitting the ^{11}B growth curves, T_C is the thickness of the target in terms of carbon nuclei, λ is the decay constant of ^{11}C, and N_p is the number of protons detected by the dE-E proton telescope. The fraction (N_p/N_n) is the calculated number of protons detected for a given number of neutrons hitting the polyethylene. This value has been computed from the geometry of the system, using the known cross sections for the $^{1}H(n, p)$ [14, 15] and $^{3}H(d, n)^{4}He$ [16] reactions.

To determine the number of ^{11}C nuclei present in the sample, the ^{11}B growth curve was fit with

$$R(t) = R_0(1 - e^{-\lambda t}) + At + B\,, \tag{14}$$

where R(t) is the integrated number of beta-decay events, R_0 is the total number of ^{11}C decays detected in the target, and At+B is the integrated background gamma radiation. Using this fit, this number of ^{11}C present in the sample is

$$N_{11C} = \frac{R_0 e^{-\lambda t_{trans.}}}{\varepsilon}\,, \tag{15}$$

where $t_{trans.}$ is the time of transport between irradiation with high-energy neutrons and the start of beta-decay counting. The only unknown value in Equation 15 is the absolute full-peak efficiency of the

detectors, ε. Determining this value is the subject of this thesis and must be known before an accurate cross section can be measured.

2.2 Efficiency for a Single NaI Detector

Methods for theoretically calculating the efficiency of NaI detectors were tested against measurements in simplified geometry so that a mathematical model of the counting station and targets used in the Ohio University experiment could be validated. Several small experiments were carried out at Houghton College to measure the full-peak coincidence efficiency to within 5%, which was then used to validate the model for various geometries, materials, and radioactive sources. After the model was validated, it was used to calculated efficiencies for the Ohio University Experiment.

The Monte-Carlo technique was used to calculate the theoretical efficiency in each method except for the integral model described in Section 2.2.1. These Monte-Carlo calculations use an algorithm to create pseudorandom vectors, which simulate the paths of particles involved in the experiment, including positrons and gamma rays. In each method, the materials through which the particles may travel are simulated. This allowed for a theoretical calculation of particle interactions with these materials, including the likelihood of a particle being measured by the detectors, which, as stated earlier, is never 100%.

2.2.1 Integral Modeling of Efficiency

The absolute singles efficiency was calculated by an integral developed from Ref [17] that treated gamma rays emitted by positron annihilation as coming from a point source, directly along the axis of the cylindrical detector

$$\varepsilon = \int_0^{\theta_1} \frac{\left(1\text{-}e^{-\mu\frac{H_d}{\cos\theta}}\right)\sin\theta d\theta}{1\text{-}\cos\theta_0} + \int_{\theta_1}^{\theta_0} \frac{\left(1\text{-}\,e^{-\mu\left(\frac{R_d}{\sin\theta}\text{-}\frac{d}{\cos\theta}\right)}\right)\sin\theta\, d\theta}{1\text{-}\cos\theta_0} \tag{16}$$

where μ is the attenuation coefficient of the detector material, H_d is the height of the detector, θ is the angle of the gamma ray's path from the symmetric axis of the cylindrical NaI detector, R_d is the radius of the detector, and d is the distance between the source and the detector face as shown in Figure 7.

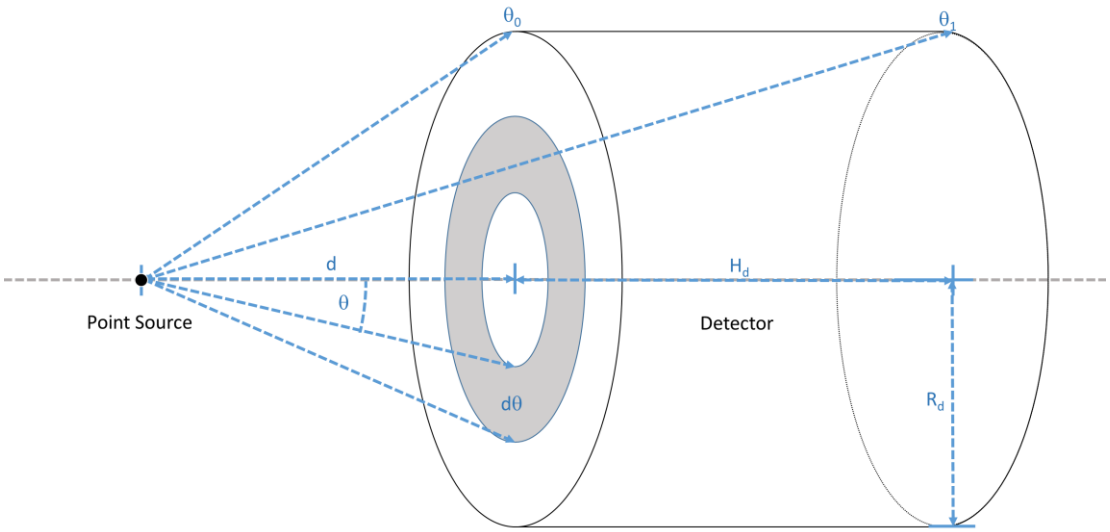

Figure 7. Diagram of the parameters for the integral model of calculating efficiency showing the distance between the source and detector face, d; the height of the detector, H_d; the trajectory of the photon, θ; and trajectories to the edge of the detector at both the upstream and downstream faces, θ_0 and θ_1, respectively.

2.2.2 Simple Monte-Carlo Modeling of Efficiency

Modeling the efficiency using an extended source rather than a point source was necessary to develop an accurate simulation of the disk sources used in the experiment. To simulate a disk source with material around it, a simple Monte-Carlo code was written using the techniques described in Ref [18]. For this code, which is included in Appendix A.1, gamma rays were emitted isotropically into a hemispherical volume inside of which a detector was simulated.

The user was able to define the geometry of the simulation, the attenuation coefficient of each material, the number of gamma rays simulated, and the energy of those gamma rays. The model used a random floating point value between 0 and 1, q, which was independently calculated for each instance it was used. Figure 8 is a diagram this simulation.

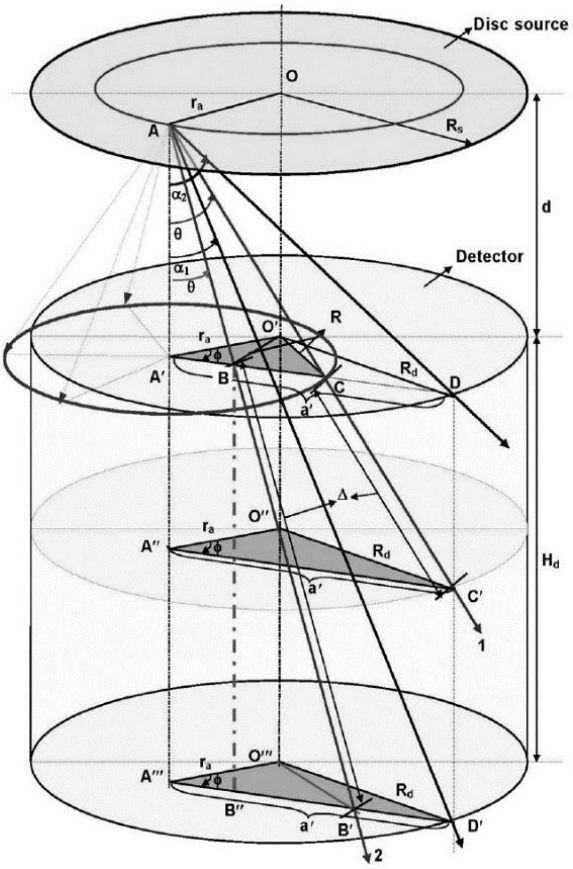

Figure 8. Diagram of the Monte-Carlo model for calculating efficiency. Simulated gamma rays are allowed to originate at any point within the defined cylindrical region, disk source. These gamma rays are given a random direction by the code and their paths are used to calculate the likelihood of their interaction in the detector. Figure from Ref. [18].

To generate the location of a decay event, radius r_a, between the origin point and the center of the disk source was set to

$$r_a = R_s \sqrt{q}\,, \tag{17}$$

where R_S is the radius of the source.

The direction of gamma ray emission is determined by θ and Φ which were set to

$$\theta = \cos^{-1}(q) \tag{18}$$

and

$$\Phi = 2\pi q\,, \tag{19}$$

where θ is the angle between the path of the gamma ray and the axis of the detector and Φ is the azimuthal angle of the ray.

If the code determined from these values that the path of the gamma ray would not intersect with the NaI detector, the simulated ray was marked as not measured by the detector. However, if the path of the gamma ray did intersect with the detector, the code calculated the likelihood that the gamma ray was counted by the detector

$$S(E) = 1 - e^{-\mu(E)\Delta}\,, \tag{20}$$

where S is the likelihood of the detector counting the simulated ray, μ(E) is the attenuation coefficient of the detector, and Δ is the distance the gamma ray travels through the detector. The likelihood that the gamma ray was counted by the detector increases with the distance that ray travels within the detector. Figure 9 is a diagram output from the simple Monte Carlo code simulating a coincidence efficiency measurement.

Here, it is assumed that if the gamma ray interacts in any way in the detector, it is detected. Hence, the likelihood is overestimated. Also, this code only gives the total efficiency and must be corrected using an experimentally measured ratio of full peak to total gamma rays. This code did not include the effects of Compton scattering and was unable to deal with the more complex geometries found in latter experiments.

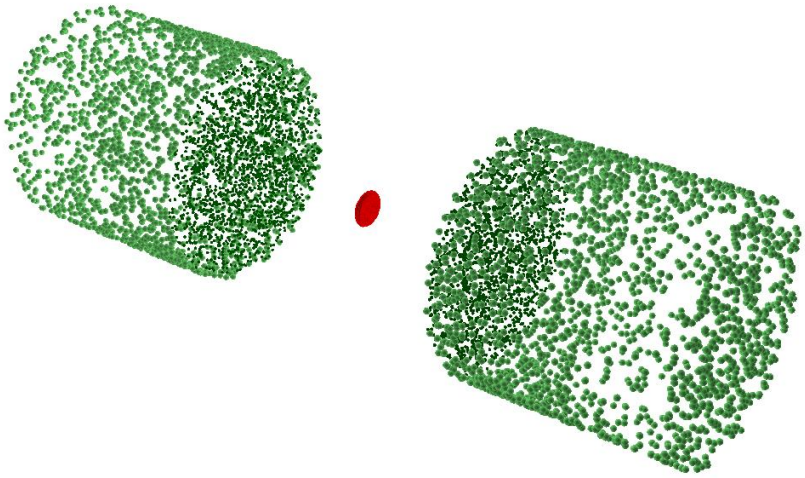

Figure 9. Output diagram from the simple Monte-Carlo. Simulated gamma rays are emitted (red points) and can enter the NaI detectors (dark green points) and exit with the same trajectory (light green points). Probability of detection is calculated from the distance traveled through the detectors.

2.3 Coincidence Efficiencies Using GEANT

To fix these problems, another Monte-Carlo code was written using Geant4 subroutines. This code allowed for a more accurate simulation of the materials surrounding the source as well as Compton scattering of the gamma rays in the material. The GEometries ANd Tracking (GEANT) platform simulates particle paths through matter. It has reference libraries of element properties, radiation decay schemes, and other material data. The codes developed to calculate the coincidence efficiency were written in C++. The simulations were developed from work done by Dr. Ryan Fitzgerald in the Radiation Physics division at the National Institute of Standards and Technologies (NIST). Sections of the code are included in the Appendix.

A GEANT simulation was written for each of several experiments and validated by testing how closely it compared to the measured efficiency. Each simulation code consisted of sixteen C++ files and their

corresponding header files as shown in Table 1. The header files contained variable declarations as well as setter and getter methods for the C++ files.

Materials in the code were compounds of elements included in GEANT libraries. The materials were created in "LTAC1DetectorConstruction.cc" using values of density and information about material composition from NIST. Appendix A.2.1 contains the code used to create the simulated compounds. The geometry of each experiment was also included in "LTAC1DetectorConstruction.cc".

Table 1. C++ and header files for GEANT. Each C++ file has a corresponding header file in which variables are declared along with setter and getter methods.

PhysicsList.hh	PhysicsList.cc
StepMaxMessenger.hh	StepMaxMessenger.cc
PhysicsListMessenger.hh	PhysicsListMessenger.cc
PhysListEmStandard.hh	PhysListEmStandard.cc
StepMax.hh	StepMax.cc
LTAC1StackingActionMessenger.hh	LTAC1StackingActionMessenger.cc
LTAC1RunAction.hh	LTAC1RunAction.cc
LTAC1RunActionMessenger.hh	LTAC1RunActionMessenger.cc
LTAC1PrimaryGeneratorAction.hh	LTAC1PrimaryGeneratorAction.cc
LTAC1Hit.hh	LTAC1Hit.cc
LTAC1StackingAction.hh	LTAC1StackingAction.cc
LTAC1DetectorConstruction.hh	LTAC1DetectorConstruction.cc
LTAC1EventAction.hh	LTAC1EventAction.cc
LTAC1SD.hh	LTAC1SD.cc
LTAC1Analysis.hh	LTAC1Analysis.cc
EmPenelopePhysics.hh	EmPenelopePhysics.cc

During a simulation, decay events were handled individually with the position and reactions of emitted particles evolving through time-stepping. Multiple particles evolved in each time-step. In each step, the particles underwent interactions with the simulated materials including Compton scattering and ionization based on definitions of physical interactions included in the code. Parameters for the emission

of decay particles, including their start position, direction, and energies were set in "LTAC1PrimaryGeneratorAction.cc" which is included in Section A.3.

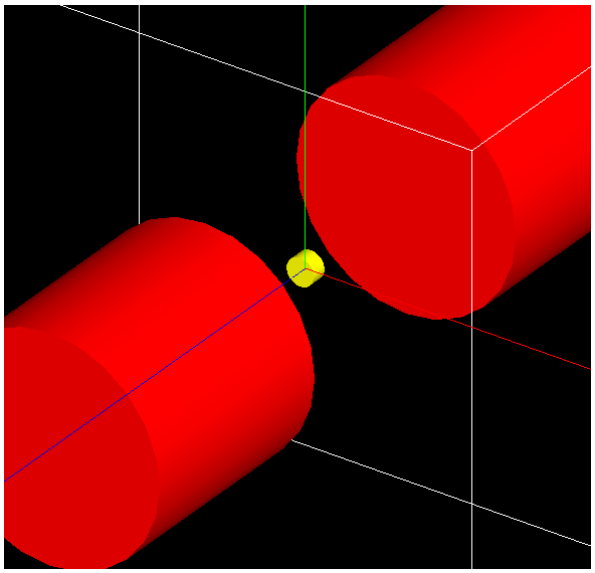

Figure 10. Output diagram from the GEANT Monte Carlo for a simulation of Experiment IV.

GEANT produced a calculated energy spectrum where the number of gamma rays that interacted in the detectors were plotted with respect to the energy they deposited in the detector. Figure 11 is an example spectrum produced by GEANT for a positron disk source near a single NaI detector. The code will output energy spectra for both singles and coincidence. The absolute total singles and coincidence efficiencies were calculated by dividing the number of gamma rays detected in each spectra by the number of positron-emitting events in that simulation. The absolute full-peak singles and coincidence efficiencies were calculated by dividing the number of gamma rays detected in the full-peak in each spectra by the number of positron-emitting events in that simulation. After the code was validated as predicting the measured efficiency to within 5%, it was used to calculate the efficiencies for the Ohio University Experiment. These were used to calculate the $^{12}C(n, 2n)^{11}C$ cross section.

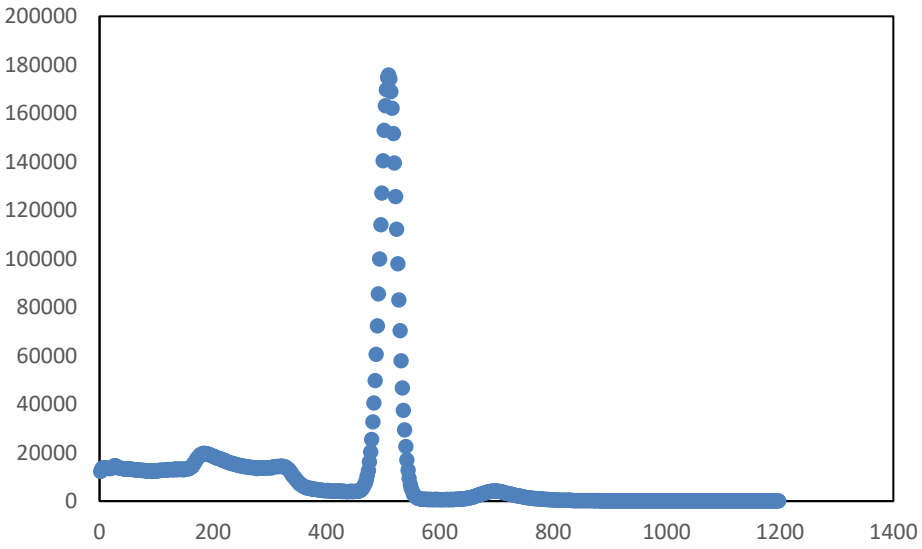

Figure 11. GEANT-calculated energy spectrum for a positron disk source close to a NaI detector. The frequency of gamma rays is plotted as a function of their energies.

Chapter 3

MEASURED EFFICIENCY OF SODIUM IODIDE DETECTORS

Six experiments were performed to validate simulations used to calculate the efficiencies of the NaI detectors. In each experiment, a source emitted a known number of positrons, which annihilated to produce back-to-back 511 keV gamma rays. These gamma rays were measured by NaI detectors from the Ohio University Experiment. Using spectra produced by these measurements and the number of positrons from the source, the efficiency was calculated as the fraction of total gamma rays the detectors measured.

Experiment I tested the associated particle method of counting positron emissions, used to measure the efficiency of the detectors. Experiment II improved this by removing summing events from the data. These experiments both measured the efficiency for only one detector. The first experiment that measured coincidence efficiency was Experiment III. This method was modified in Experiment IV to reduce both Compton scattering near the source and asymmetries in the experimental apparatus. A different technique, using a calibrated source was used in Experiment V. Graphite disks near the source were added in Experiment VI to test how well the effects of Compton scattering could be calculated by the GEANT simulation.

3.1 Experiment I: Preliminary Measurement

Experiment I was a measurement of efficiency for a single NaI detector. Figure 12 is a diagram of this experiment. Figure 13 is a diagram of the electronics for the experiment. Approximately 1 μCi of ^{22}Na was evaporated into a shallow indentation on a 0.7 mm thick polyethylene disk. The ^{22}Na decayed into an excited state of ^{22}Ne by emitting a positron. The ^{22}Ne de-excited by releasing a 1275 keV gamma ray. An ORTEC BA-024-025-1500 silicon surface barrier (SSB) detector with 1500 μm depletion depth and an active area of 25 mm^2 detected the positrons emitted by the ^{22}Na. Gamma rays from positron annihilation in the SSB were detected by an ORTEC 905-4 NaI detector with an active diameter of 7.62 cm and a height of 7.62 cm (3 inches by 3 inches). This was one of the same detectors used to count positron annihilation events in the Ohio University Experiment. It will be referred to henceforth as Detector I.

Some positrons from the ^{22}Na annihilated in the silicon surface barrier and produced electronic pulses. A fraction of the 511 keV gamma rays produced by these annihilations entered the NaI detector and ionized the NaI crystal. This produced electronic pulses with amplitudes proportional to the energy of the gamma ray measured.

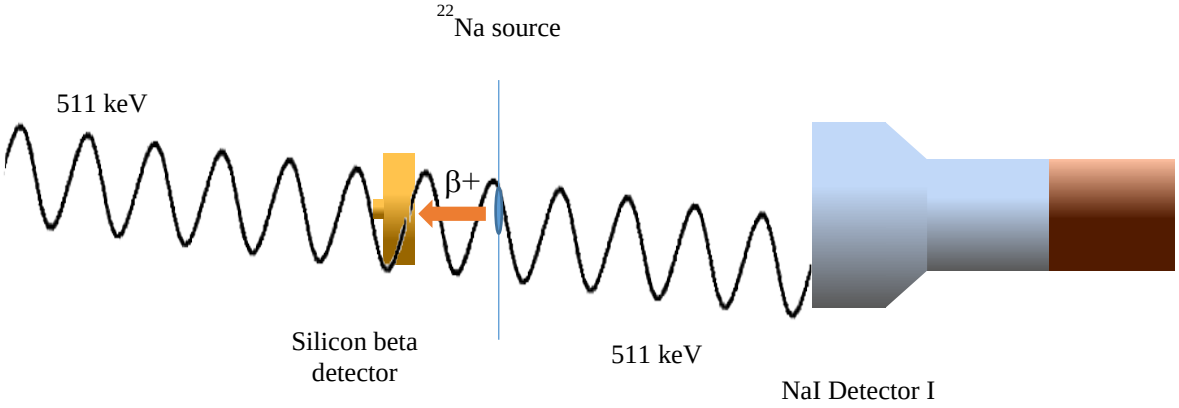

Figure 12. Diagram of the apparatus for Experiment I. Positrons from the ^{22}Na source annihilate in the silicon beta detector. This annihilation produces back-to-back 511 keV gamma rays that can enter NaI Detector I and be measured.

The pulses from Detector I were amplified by an ORTEC 485 spectroscopy amplifier and events in the 511 keV peak were selected using an ORTEC 551 timing single-channel amplifier (TSCA). The logic pulse from the TSCA was delayed by an ORTEC 416A gate generator and started the time-to-amplitude converter (TAC) ORTEC 437. This was chosen as the start pulse because of its lower pulse rate.

The pulses from the silicon surface barrier detector were sent through an ORTEC 142 pre-amplifier, an ORTEC 485 spectroscopy amplifier, to an ORTEC 551 TSCA. The pulse from the TSCA stopped the ORTEC 437 TAC. This was chosen as the stop pulse because its pulse rate was faster than Detector I.

The TAC output an analog pulse with amplitude proportional to the time difference between the start pulse from the NaI detector and the stop pulse from the silicon surface barrier detector for each event. Pulse amplitudes from the TAC were digitized by a Spectech UCS30 multichannel analyzer (MCA). The

resulting histogram was recorded by a computer running Windows XP. Pulses from the TAC for which both detectors were triggered within 610 ns were selected by the ORTEC 550 single channel analyzer (SCA) and output to a Mech-Tronics 715 dual scaler, which counted the number of coincidence events. The FWHM of the coincidence peak was 265 ns.

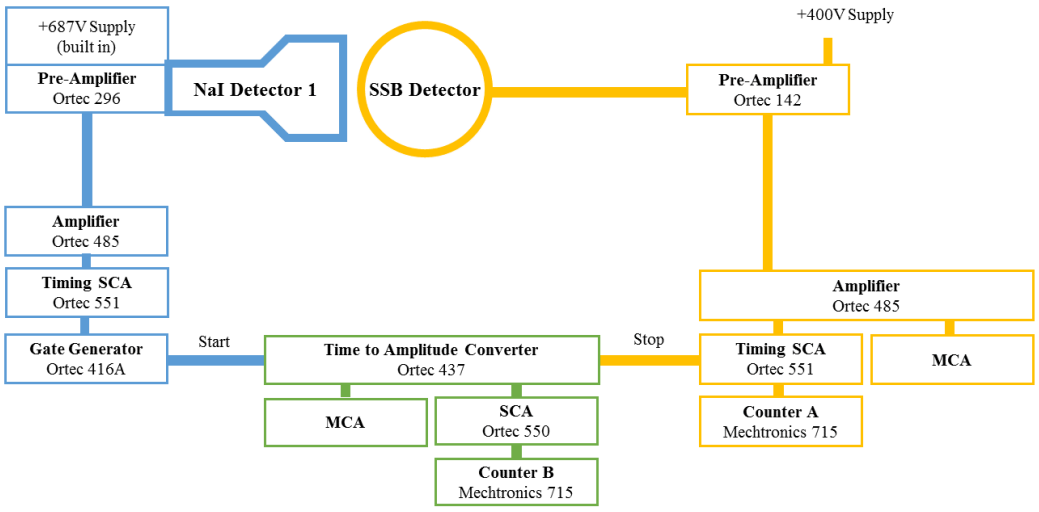

Figure 13. Diagram of the electronics used in Experiment I to make a preliminary measurement of the singles efficiency of NaI Detector I. Electronic pulses from the detectors were amplified and events in the 511 keV peak were selected by a TSCA. The time difference between when the positron was emitted and measured was recorded by a TAC. Pulses from the silicon detector and Detector I were recorded in an MCA. Counter A records the number of 511 keV gamma rays detected. Counter B records the number of coincidences of 511 keV gamma rays and positrons detected.

3.1.1 Efficiency Measurements for Experiment I

The absolute full-peak efficiency for the experiment was

$$\varepsilon = \frac{N(511\ \text{keV} \cdot \beta)}{N(\beta)} \tag{21}$$

where ε is the absolute full-peak efficiency, N(511 keV · β) is the number of coincidences between Detector I and the silicon detector as recorded by Counter B, and N(β) is the number of positrons that annihilated in the silicone surface barrier detector as reported by Counter A. Positrons that annihilated outside of the silicon surface barrier detector do not affect this measurement because the efficiency is measured as the fraction of events where a gamma ray is detected for a beta-decay event that triggered the silicon detector.

The integral method from Section 2.2.1 and the simple Monte-Carlo method from Section 2.2.2 were used to calculate efficiency values for this experiment. The Monte-Carlo calculated the absolute total efficiency for the Detector I. In order to find the absolute full-peak efficiency, a ratio of full-peak events to total events was experimentally measured. This ratio was found to be roughly 0.63 and was used to calculate the absolute full-peak efficiency. In addition to this, the absolute full-peak singles efficiency was simulated by normalizing the absolute total singles efficiency calculated by the simple Monte-Carlo to the measured absolute full-peak singles efficiency at 10 cm.

When these values were compared to the experimentally measured values for efficiency it was found that the calculation over-predicted the absolute full-peak efficiency. Figure 14 is a plot of the experimentally measured and calculated efficiency values. A value of absolute full-peak singles efficiency from ORTEC for Detector I is also plotted [19].

3.1.2 Summing Events

It was hypothesized that the difference between the calculated and measured efficiencies was caused by 1275 keV de-excitation gamma rays from the source summing with 511 keV gamma rays in the NaI

detector as shown in Figure 15. This shifted the 511 keV gamma rays out of the full-peak, artificially lowering the measured values of efficiency. The simple Monte-Carlo did not account for this effect.

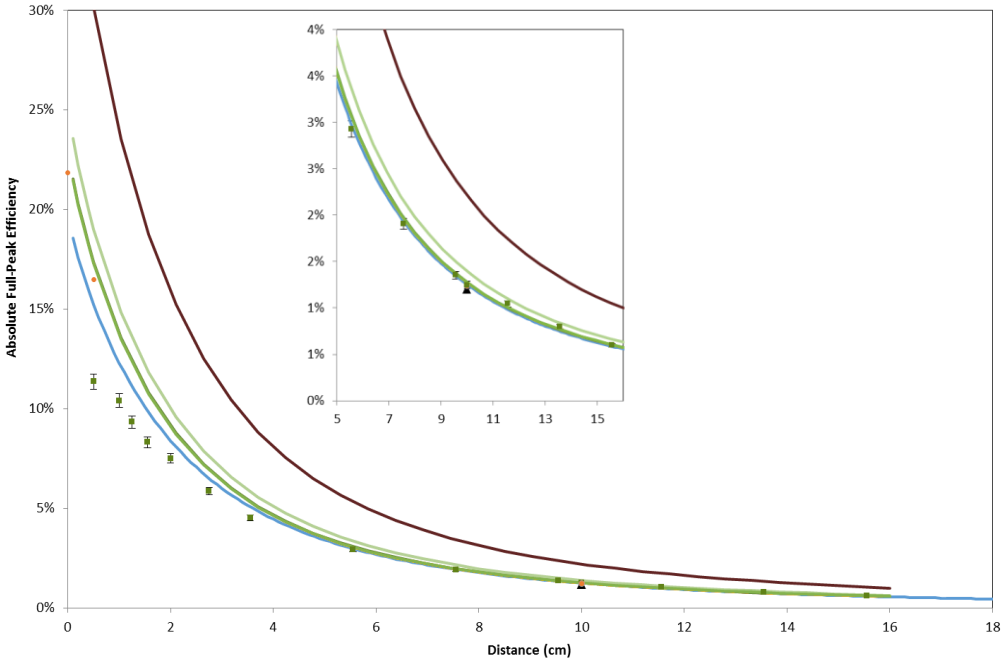

Figure 14. Plot of absolute singles efficiency for Experiment I as a function of the distance between the NaI and SSB detectors including the experimentally measured full-peak (green squares), manufacturer's value for the full-peak from Ref [19] (brown triangle), previous measurements (orange circles), the full-peak calculated by the integral method in Section 2.2.1 (blue curve), calculations by the Monte-Carlo Method in Section 2.2.2 for the total (brown curve), the total normalized to 10 cm (dark green curve), the full-peak efficiency with a full-peak to total efficiency ratio of 0.63 (light green curve), and the efficiency for a simulated disk-source normalized to 10 cm (green curve).

The probability that 1275 keV and 511 keV gamma rays summed together in the NaI detector was greater when the source and detector were closer together. Therefore, the effect was more pronounced at smaller distances and produced the greater difference between the calculated and measured values, which were observed.

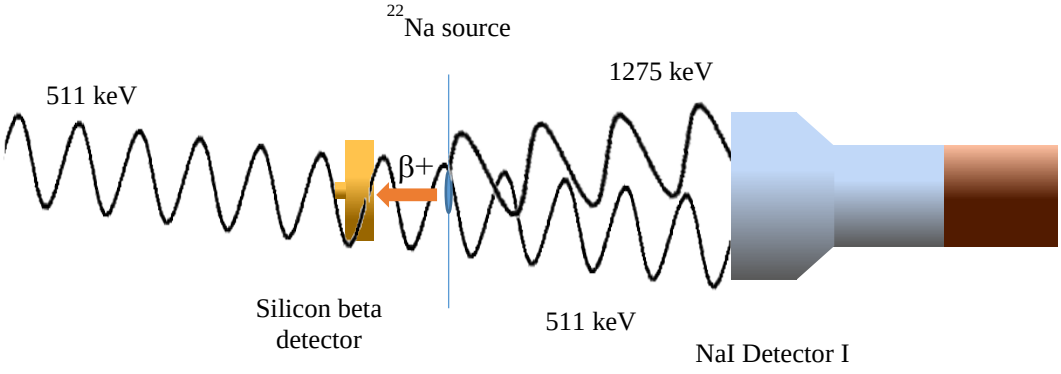

Figure 15. Diagram of 1275 keV and 511 keV gamma rays summing in Experiment I. The 1275 keV gamma rays are produced by the de-excitation of daughter nuclei from ^{22}Na and add to the energy of 511 keV gamma rays, shifting them out of the full-peak and lowering the absolute full-peak singles efficiency.

3.2 Experiment II: Vetoing Summing Events

The experimental apparatus was altered to eliminate the effects of 1275 keV and 511 keV gamma summing together. To correct for the summing effects, a Bicron 693-000102 NaI detector was added to the experiment with its center axis perpendicular to the center axis of Detector I and coaxial with the silicon surface barrier detector as shown in Figure 16. This 7.62 cm diameter by 7.62 cm height cylindrical detector with a 2.22 cm wide by 3.54 cm deep well will be referred to as the "Veto" detector.

If the "Veto" detector is measuring a 1275 keV gamma ray, the ray cannot be present in Detector I at the same time as a 511 keV gamma ray and summing of the de-excitation and full-peak gamma rays cannot occur. Because the timing of the detectors is much faster than the rate of decay of the ^{22}Na there is no possibility that more than one de-excitation gamma ray will be released and fool the "Veto" detector.

For a gamma ray to be measured in Detector I, it was required to be detected simultaneously with a 1275 keV gamma ray in the "Veto" detector. This absolute full-peak efficiency was

$$\varepsilon = \frac{N(511\ keV \cdot \beta \cdot "Veto")}{N(\beta \cdot "Veto")} \tag{22}$$

where N(511 keV · β · "Veto") is the number of coincidences between a 511 keV gamma ray in Detector I, a positron in the silicon detector, and 1275 keV in the "Veto" detector. The term N(β · "Veto") is the number of coincidences between a positron in the SSB detector and 1275 keV in the "Veto" detector.

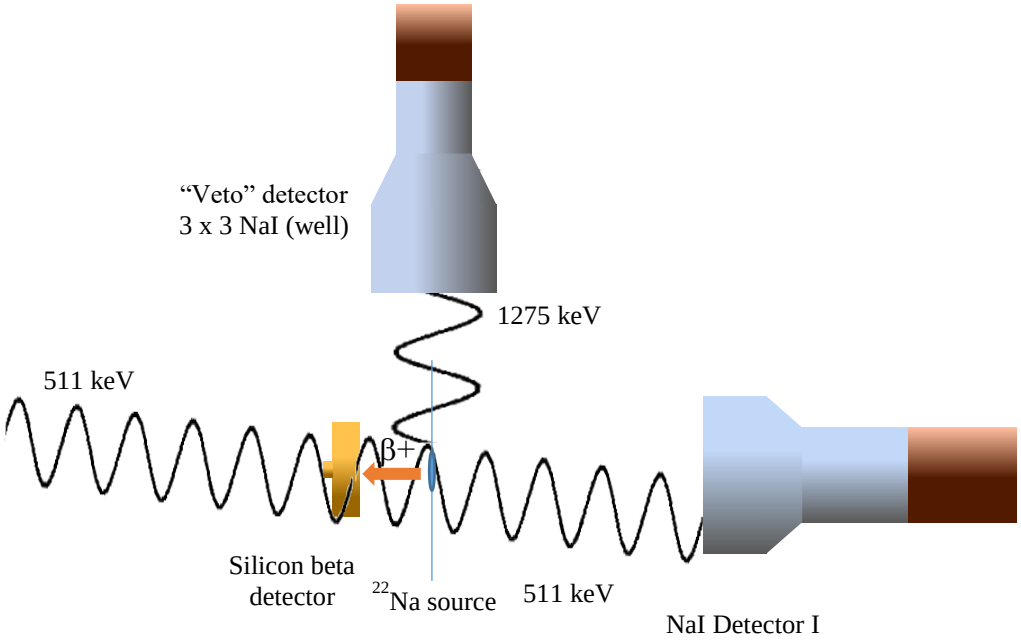

Figure 16. Diagram of the experimental apparatus for Experiment II. The ^{22}Na, SSB detector, and Detector I are the same as in Experiment I. This experiment adds a "Veto" Detector, which prevents summing events in Detector I.

3.2.1 Electronics for Experiment II

This experiment corrected the measured efficiency by ensuring that the 1275 keV de-excitation gamma rays were not in Detector I with a 511 keV gamma ray. Gamma rays measured by Detector I were only recorded if the "Veto" Detector measured a 1275 keV gamma ray at the same time. The FWHM of the

coincidence timing spectrum was about 250 μs, which is shown in Figure 17. This required timing electronics that were more advanced than those used in Experiment I. A Jorway 73A Computer Automated Measurement and Control (CAMAC) system was used to handle the electronic pulses from the apparatus instead of an MCA. The CAMAC system can record a large number of parameters on an event-by-event basis. The data were analyzed and histograms were produced using a custom C++ code implemented using SJY CAMAC drivers from Fermilab [20] and the ROOT data analysis framework [21]. Figure 18 is a diagram of the electronics used for Experiment II. Pulses emitted from the detectors were sent to ORTEC 485 amplifiers.

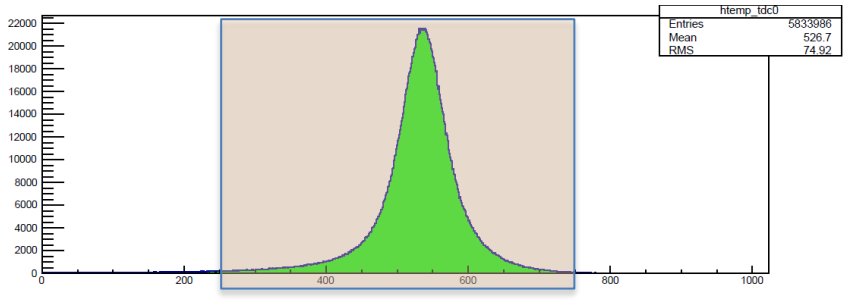

Figure 17. Histogram of the time difference between the timing pulse from the SSB detector and the NaI detector. The x-axis is channels. FWHM of the coincidence peak is about 250 μs. The shaded box represents the cut that was applied to select good coincidence events.

The pulses from the amplifiers for Detector I and the "Veto" Detector that corresponded to gamma rays in the 511 keV and 1275 keV energy peaks respectively, were selected by ORTEC 551 TSCA modules which produced logic timing pulses for these events. The LeCroy 3377 TDC was started by a logic timing pulse from the silicon surface barrier detector and stopped by pulses from the Detector I and the "Veto" Detector. After the TDC was stopped, a LeCroy 2323A gate generator deactivated the circuit for 20 μs, which gave the system time to convert the pulses from analog to digital and transfer data to the CAMAC. The pulse heights were digitized using an ORTEC 413AD analog-to-digital converter (ADC). The 7 μs gate for the ADC was created by the logic pulse from the silicon surface barrier detector. The logic pulses from each detector were counted by a LeCroy 2551 scaler.

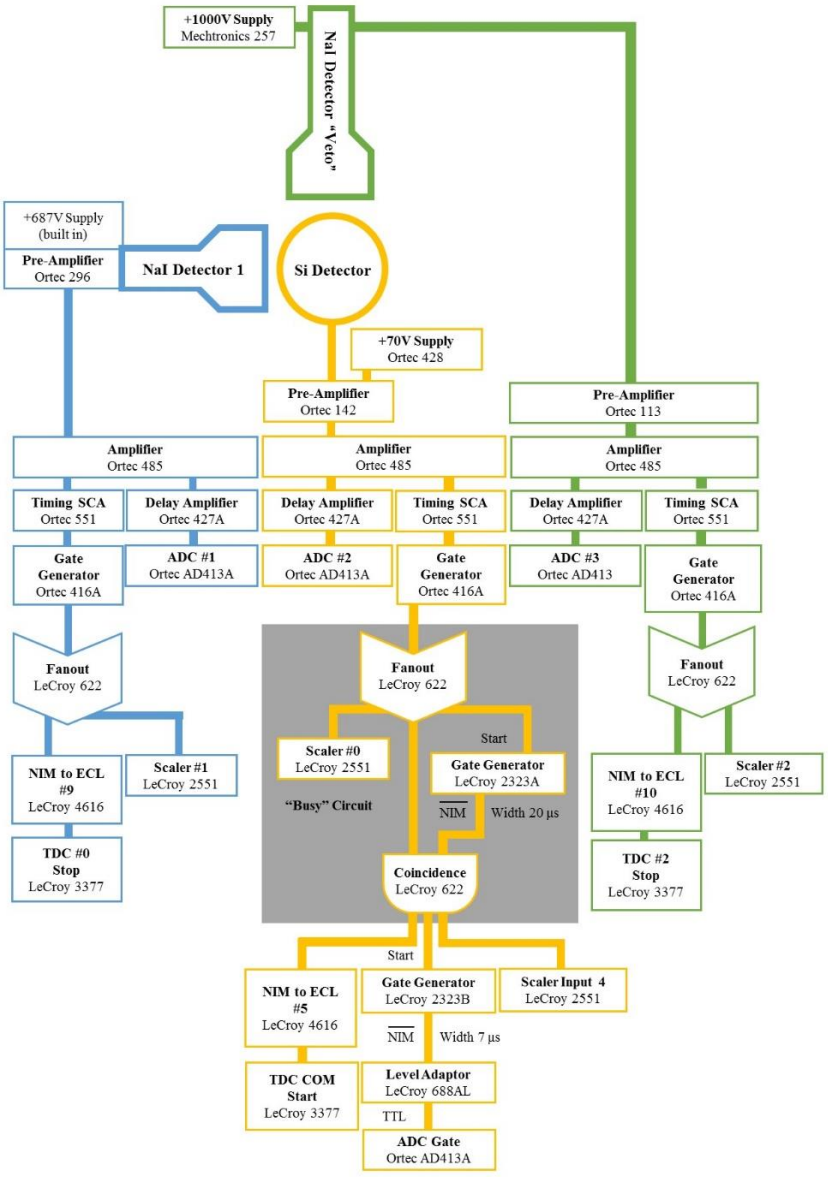

Figure 18. The electronics for Experiment II. Electronic pulses from the detectors were amplified and those corresponding to gamma rays measured by Detector I in the 511 keV energy peak were selected by a TSCA. Gamma rays measured by the "Veto" Detector in the 1275 keV energy peak were also selected so that Detector I only made a measurement when a 1275 keV gamma ray was in the "Veto" Detector. A TDC was started by the pulse from the SSB detector and stopped by the pulses from Detector I and the "Veto" Detector to measure the time difference between measurements in these detectors.

3.2.2 Efficiency Measurements for Experiment II

For Experiment II, calculated and measured efficiency values agreed better than they did for Experiment I when summing events were removed. A calculation of efficiency for this experiment was produced by the Monte-Carlo code discussed in Section 2.2.2. The efficiency was found as a function of the distance between Detector I and the ^{22}Na source. Figure 19 is a plot of the absolute full-peak efficiency.

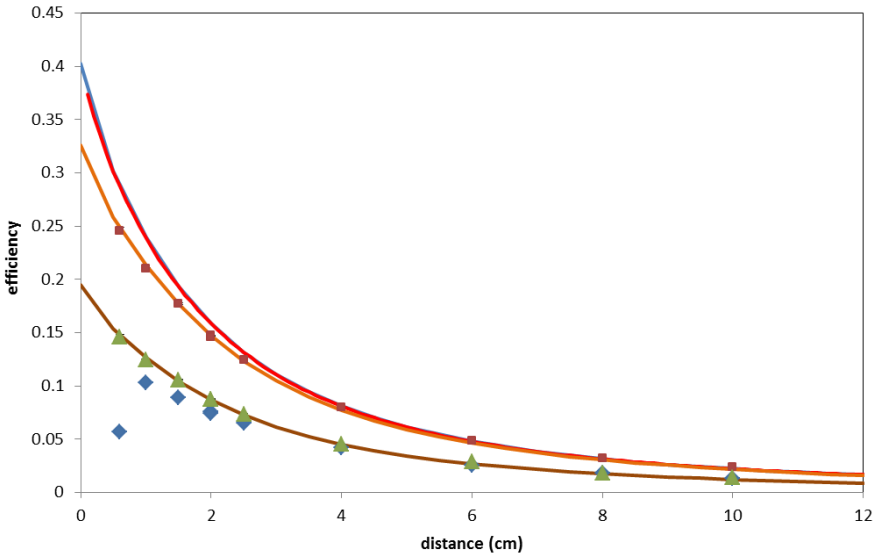

Figure 19. Plot of efficiency as a function of distance between Detector I and the ^{22}Na source for Experiment II including the measured absolute full-peak efficiency without correction to eliminate summing events (blue diamonds), measured absolute full-peak efficiency with summing errors removed (green triangles), measured absolute total efficiency with summing errors removed (brown squares), calculated absolute total efficiency using the integral method described in Section 2.2.1 (blue curve), calculated absolute total efficiency using a Mathcad method not covered in this paper (red curve), calculated absolute total efficiency using the Monte-Carlo method described in Section 2.2.2 (orange curve), and calculated absolute full-peak efficiency also using the Monte-Carlo method (brown curve).

These efficiency values were only for one NaI detector measuring 511 keV gamma rays. What was needed to find the ^{12}C(n, 2n)^{11}C cross section was the absolute full-peak coincidence efficiency which required another NaI detector.

3.3 Experiment III: Efficiency in Coincidence

To measure the absolute full-peak coincidence efficiency of the detectors, another NaI detector was added to the experimental apparatus, as shown in Figure 20, coaxial with and opposite from Detector I. This new detector will be referred to as Detector II. The SSB detector was changed to a transmission mounting so that the gamma rays would not have to pass through the back of the detector. A lack of symmetry in the apparatus would make it much more difficult to accurately model in the Monte Carlo simulation. Figure 22 is a diagram of the silicon beta detector and source apparatus used in Experiment III. The electronics for Detector II were identical to those for Detector I as shown in Figure 21.

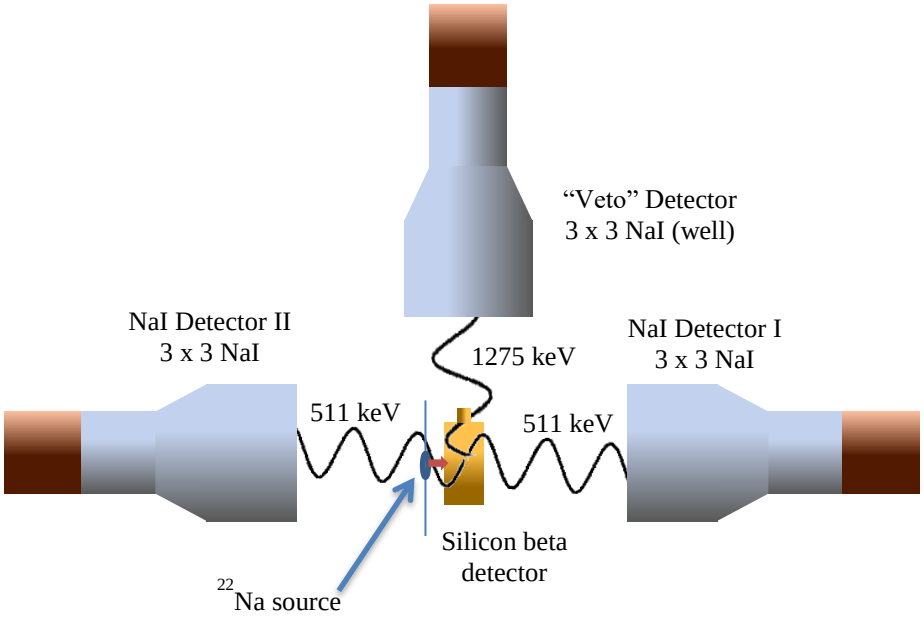

Figure 20. Set up used to measure the coincidence efficiency in Experiment III. Positrons from the ^{22}Na triggered a silicon beta detector. When these positrons annihilated in the detector, they produced back-to-back 511 keV gamma rays that could be measured in coincidence by NaI Detectors I and II. The "Veto" Detector eliminated all events where the 1275 keV de-excitation gamma ray was not measured in the "Veto" Detector.

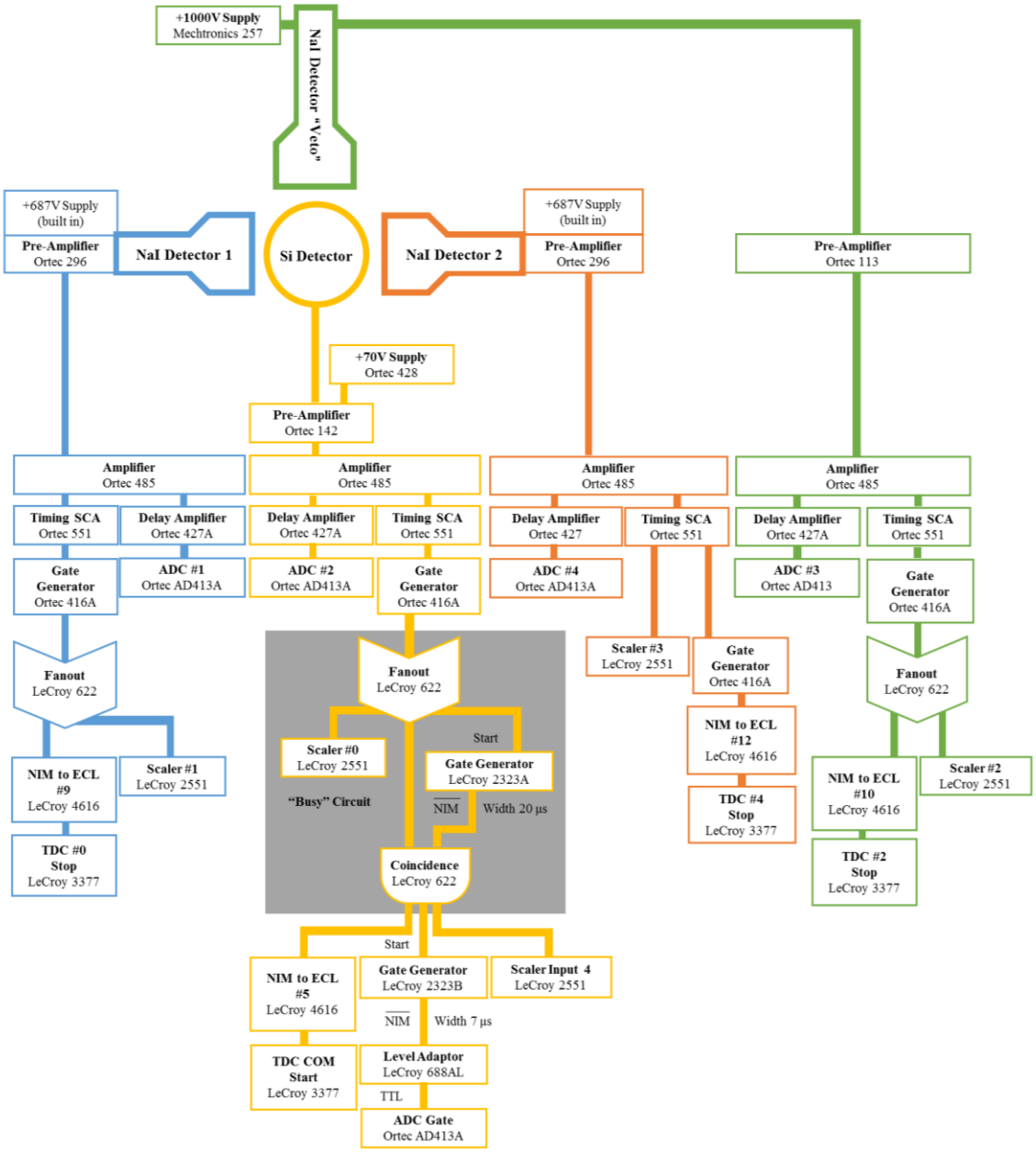

Figure 21. Electronics for Experiment III. Pulses from the four detectors were amplified and those corresponding to the 511 keV energy peak were used to stop a TDC that was started by a pulse from the silicon detector. The gamma ray energies corresponding to the pulses were sent to a CAMAC system for analysis.

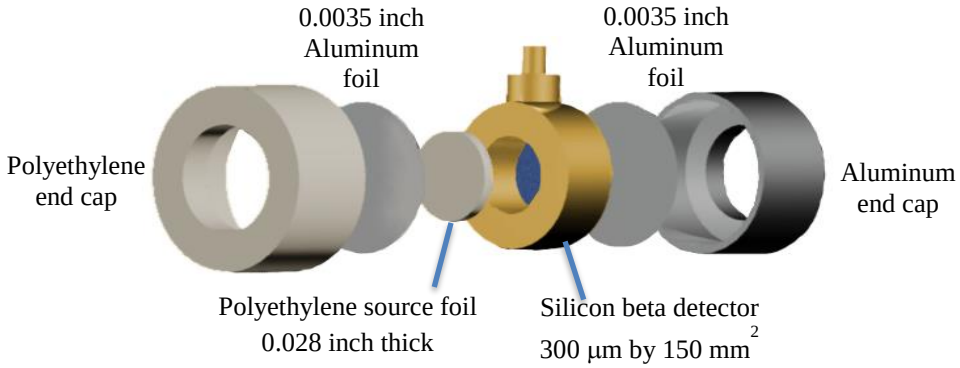

Figure 22. Source and silicon detector assembly for Experiment III. A ^{22}Na solution was evaporated onto the polyethylene source foil, which was close to the silicon beta detector. The assembly was made light tight by a layer of aluminum foil, sealed with polyethylene and aluminum end caps.

3.3.1 Efficiency for Experiment III

The absolute full-peak coincidence efficiency for the experiment was

$$\varepsilon = \frac{\mathrm{N(511\ keV\ Coincidence \cdot \beta \cdot "Veto")}}{\mathrm{N(\beta \cdot "Veto")}} \tag{23}$$

where N(511 keV Coincidence · β · "Veto") is the number of 511 keV gamma rays counted simultaneously by Detectors I and II when a positron annihilated in the SSB detector and the "Veto" detector measured a 1275 keV gamma ray. The N(β · "Veto") term is the same as in Equation 22. The absolute full-peak singles efficiency for both Detector I and II individually was also measured in this experiment. This efficiency was calculated using the same method as was used for Detector I in Experiment II.

A GEANT simulation of the experiment was developed. This code overpredicted the measured efficiencies. Figure 23 is a plot of the measured and calculated efficiencies for Experiment III. Efficiency was measured as a function of the distance between the ^{22}Na source and the faces of Detectors I and II, which were equidistant from the source.

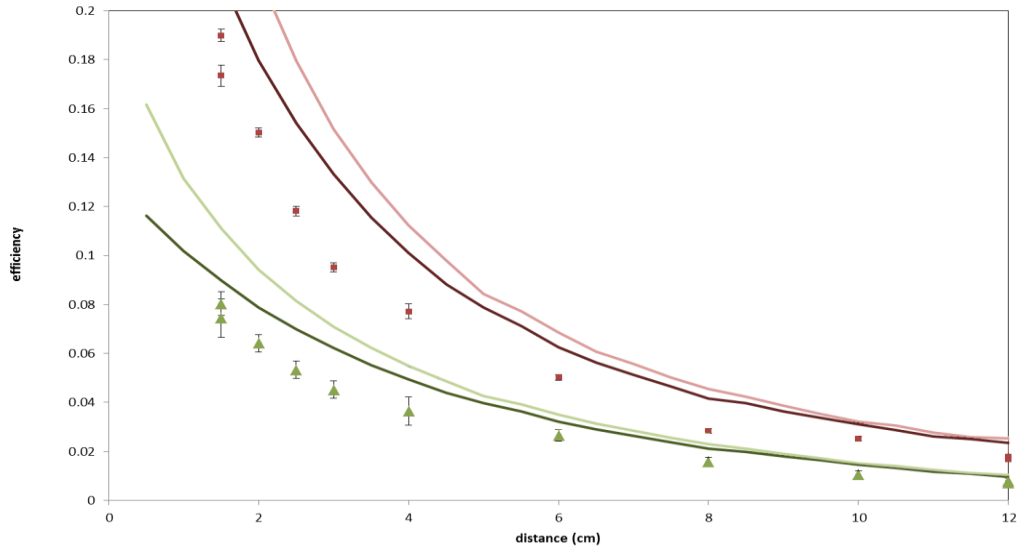

Figure 23. Plot of absolute coincidence efficiency for Experiment III as a function of distance from the face of Detectors I and II to the ^{22}Na including measured values of the efficiency (red squares) and full-peak efficiency (green triangles) as well as GEANT calculations for efficiency without attenuating material (dark red curve), efficiency with attenuating material (light red curve), full-peak efficiency without attenuating material (light green curve), and with attenuating material (dark green curve).

3.4 Experiment IV: Reduction of Attenuating Materials

The disagreement between the calculated and measured efficiencies in Experiment III was thought to possibly be caused by Compton scattering of gamma rays in the metal mount and other material surrounding the silicon beta detector. To test this hypothesis, the detector was replaced by a specially constructed plastic scintillation detector designed to minimize the material around the ^{22}Na source.

3.4.1 Design of the Scintillator Detector

The scintillator detector was constructed using BC400 polyvinyltoluene plastic scintillator and a Photonis 1-1/8 inch XP2902 photomultiplier tube (PMT) with an acrylic light guide connecting them. The scintillating plastic, shown in Figure 24, was cut to dimensions of 9.53 mm square by 5.38 mm thick, with a depression 8.6 mm square and 1.65 mm deep etched into both square faces. These wells each contained about 0.5 μCi of ^{22}Na, residue of evaporation of a weak HCl solution. Between the wells, the

plastic was 2.03 mm thick. Both faces were covered by 0.24 mm thick acrylic slides, which were held in place by ethyl-2-cyanoacrylate, standard superglue.

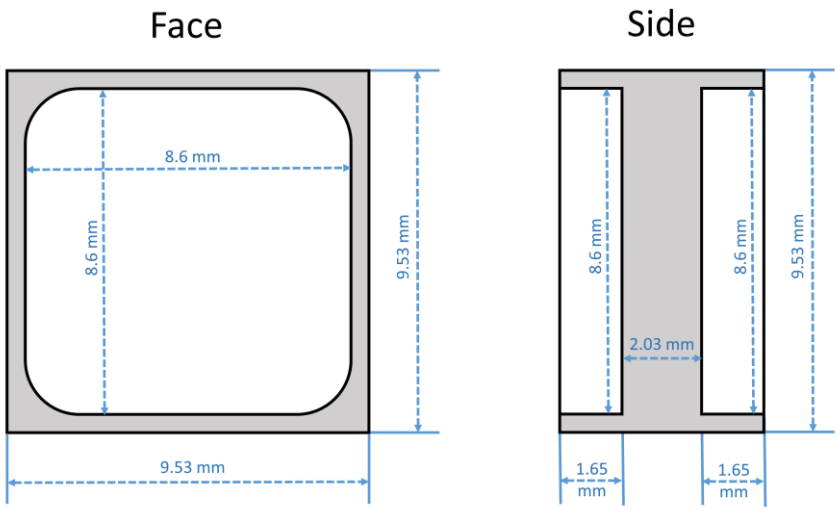

Figure 24. Diagram of the plastic scintillator used in Experiment IV. The B400 Scintillating plastic held the ^{22}Na source in depressions on its faces. The 2.03 mm of plastic between the depressions was thick enough to ensure that all positrons that passed through it annihilated yet the apparatus was kept small to reduce Compton scattering.

The acrylic light guide was 101.6 mm long with faces 9.53 mm by 5.38 mm on either end. As shown in Figure 25, the scintillator plastic and PMT were affixed to either end of the light guide. The scintillator was attached to the light guide using ethyl-2-cyanoacrylate. The light guide was held to the PMT using "Bob Smith Industries 5-Minute Quick Cure Epoxy", which was chosen for its transparency and ability to hold the acrylic to the glass face of the PMT. Acrylic stabilizers were later attached for additional strength and to align the light guide with the PMT.

Positrons released by the ^{22}Na that entered the plastic membrane between the wells on the scintillator annihilated. The positrons caused polyvinyltoluene molecules in the BC400 to emit light in the visible spectrum, which was trapped by total internal reflection in the plastic, and the light guide as well as by a reflective Teflon tape coating through which the light traveled to the PMT. A photocathode on the face

of the PMT released electrons when struck by this light. This pulse of electrons was amplified by dynodes in the tube.

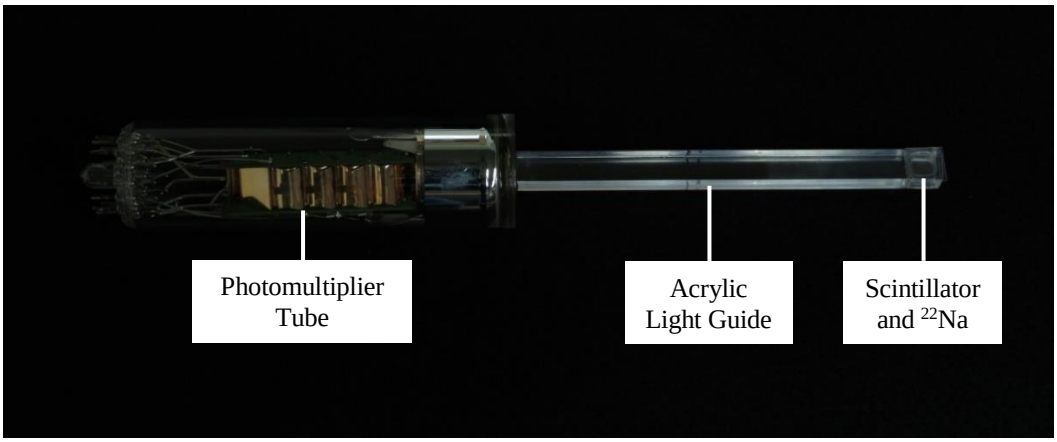

Figure 25. Scintillation detector assembly used in Experiment IV. A solution of ^{22}Na was evaporated into depressions in a scintillating plastic, which was attached to an acrylic light guide. Light was emitted by the scintillating plastic when positrons from the decay of ^{22}Na stopped in it. This light traveled down the light guide to a photomultiplier tube, which produced electronic pulses corresponding to the intensity of the light. This apparatus was wrapped with Teflon tape and electric tape to be light-tight.

Resistors, which connected dynodes, were attached to pins at the base of the PMT and created a potential difference between the dynodes, amplifying electron pulses from the photocathode. Figure 26 gives the wiring diagram of resistors and corresponding pin locations at the base of the detector, which were housed in a metal casing kept at ground. Aside from the replacement of the silicon surface barrier detector with the scintillator detector, the electronics for Experiment IV were the same as those for Experiment III.

3.4.2 Efficiency for Experiment IV

Absolute full-peak coincidence efficiency was measured using the same method as in Equation 23. Absolute full-peak singles efficiency was measured for both Detector I and II using the method in Equation 22.

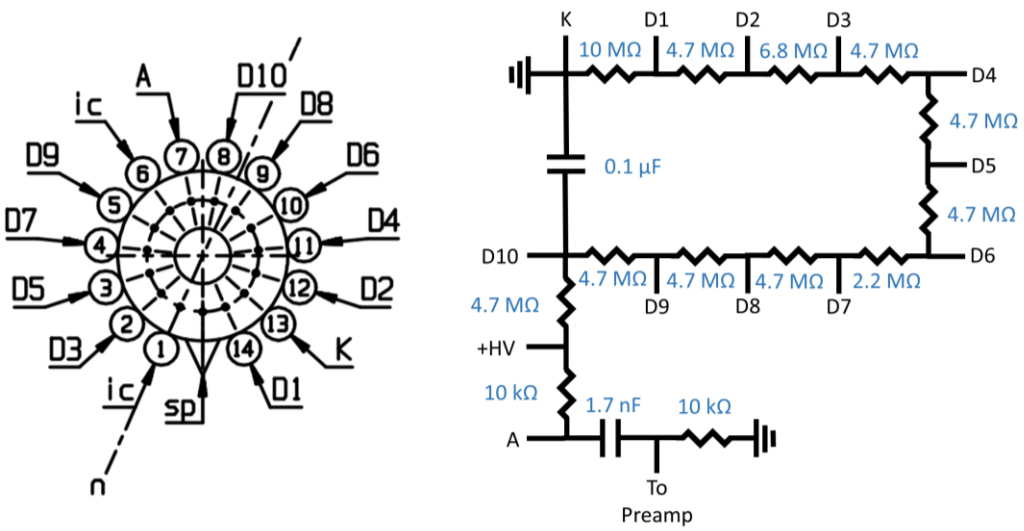

Figure 26. Voltage divider at the base of the PMT, which created potential differences between dynodes, amplifying electron, pulses from the photocathode. The left is a diagram of the pins at the base of the detector. The right is a schematic of resistors and the corresponding pins they connected.

A GEANT simulation was made to calculate the coincidence efficiency. This simulation used a precise model of Detectors I and II based on x-ray and CT scans that were made at NIST with the help of Dr. Ryan Fitzgerald. These scans revealed a 2.5 mm gap in the detectors, between the crystal and aluminum face. This space was assumed to be filled with barium oxide (BaO), which is commonly used in these applications. Figure 27 is the x-ray of Detector I. Figure 28 is an image from the CT scan of Detector I.

When the simulation was performed including such a gap, filled with BaO, the agreement between the calculated and measured efficiencies greatly improved. For absolute full-peak singles efficiency, the root mean squared (RMS) percent difference between simulation and measurement was 8.94% for Detector I and 8.31% for Detector II as plotted in Figure 29. For absolute full-peak coincidence efficiency, the RMS percent difference was 4.73% as plotted in Figure 30.

Figure 27. X-ray scan of Detector I exposed for 30 seconds at NIST, used to find a 2.5 mm gap between the crystal and face of the detector which was simulated as BaO, bringing the GEANT simulation into agreement with experimental measurement.

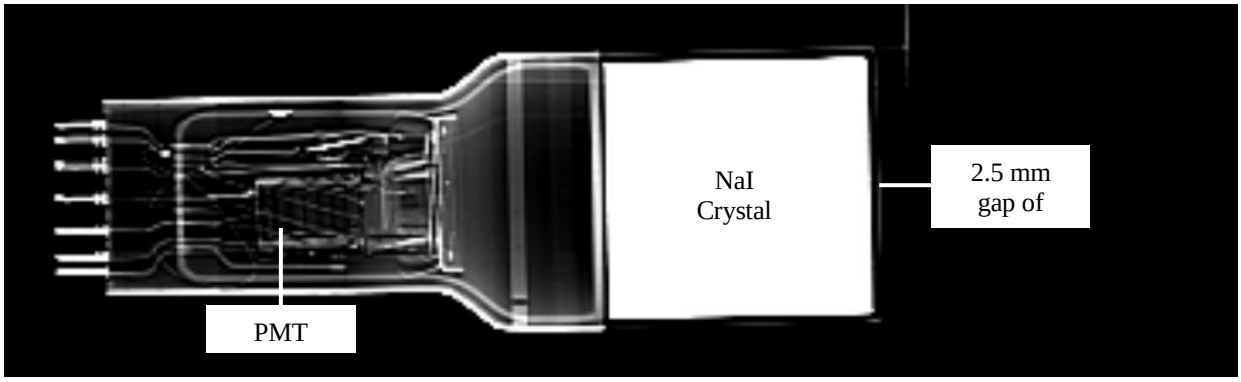

Figure 28. Image from a CT scan of Detector I taken at NIST and used to find a 2.5 mm gap between the crystal and face of the detector which was simulated as BaO, bringing the GEANT simulation into agreement with experimental measurement.

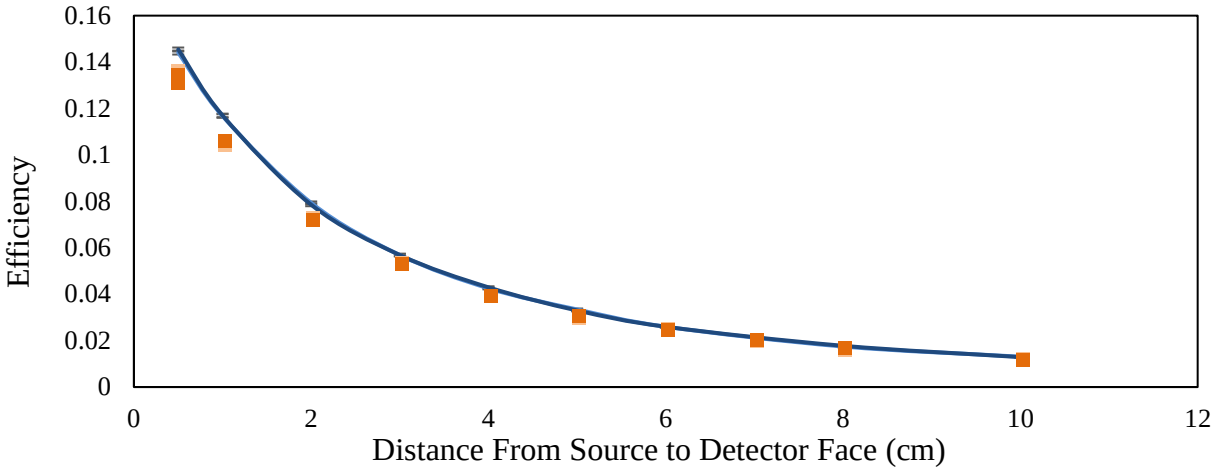

Figure 29. Plot of absolute full-peak singles efficiency for Experiment VI as a function of the distance between each Detector I and II to the ^{22}Na source including measured singles efficiency for Detector I (light orange points) and Detector II (dark orange points) as well as simulated singles efficiency for Detector I (light blue curve) and Detector II (dark blue curve). RMS percent difference for Detector I was 8.94% and 8.31% for Detector II.

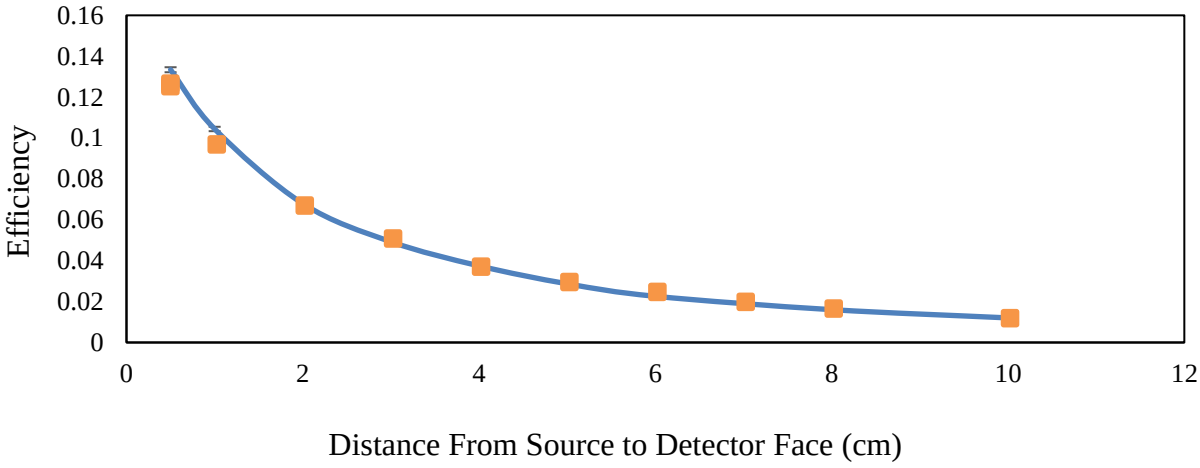

Figure 30. Plot of absolute full-peak coincidence efficiency for Experiment VI as a function of the distance between each Detector I and II to the ^{22}Na source including measured efficiencies (orange points) and the GEANT simulation (blue curve). RMS percent difference between measurement and simulation was 4.73%.

3.5 Experiment V: Calibrated ^{68}Ge Source

In this experiment, the scintillator detector and ^{22}Na source were replaced with a 0.1 μCi ^{68}Ge disk source calibrated to within 1.7% from NIST. The ^{68}Ge decays into ^{68}Ga by electron capture, which then decays by positron emission to ^{68}Zn [22]. A "Veto" detector was not needed as the source did not produce gamma rays at a rate that would cause summing issues in Detectors I and II. Because the activity for the calibrated source was known, instead of triggering on positron emissions using a detector, the efficiency was measured as

$$\varepsilon = \frac{\mathrm{N(511\ keV\ Coincidence)}}{\lambda t B} \tag{24}$$

where N(511 keV Coincidence) is the number of back-to-back gamma rays in the full peak that trigger Detector I and II within 300 ns of each other, λ is the decay constant for the source, t is time, and B is the branching ratio of the ^{68}Ga decay. The branching ratio is the fraction of total ^{68}Ga decays that occur through positron annihilation. To ensure that all of the positrons emitted by the ^{68}Ga source annihilated near the source deposit, the source was sandwiched between disks of copper as shown in Figure 31.

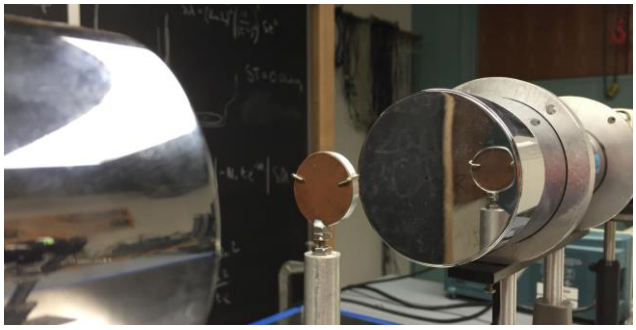

Figure 31. The set up for Experiment V showing the ^{68}Ge disk source elevated between Detectors I and II and sandwiched between disks of copper to ensure all positrons produced by the source annihilated.

The electronics for Experiment V were similar to those used in Experiment III with the SSB and "Veto" detectors removed, as shown in Figure 32. As in previous experiments, the geometry of the set up was varied by sliding Detectors I and II along their shared axis, keeping them equidistant to the ^{68}Ge source.

Additionally, for this experiment, the position of the ^{68}Ge was varied across the face of Detectors I and II, which were both 0.5 cm from the line along which the source slid. Efficiency was found with respect to the distance between the center of the disk source and the shared axis of Detectors I and II.

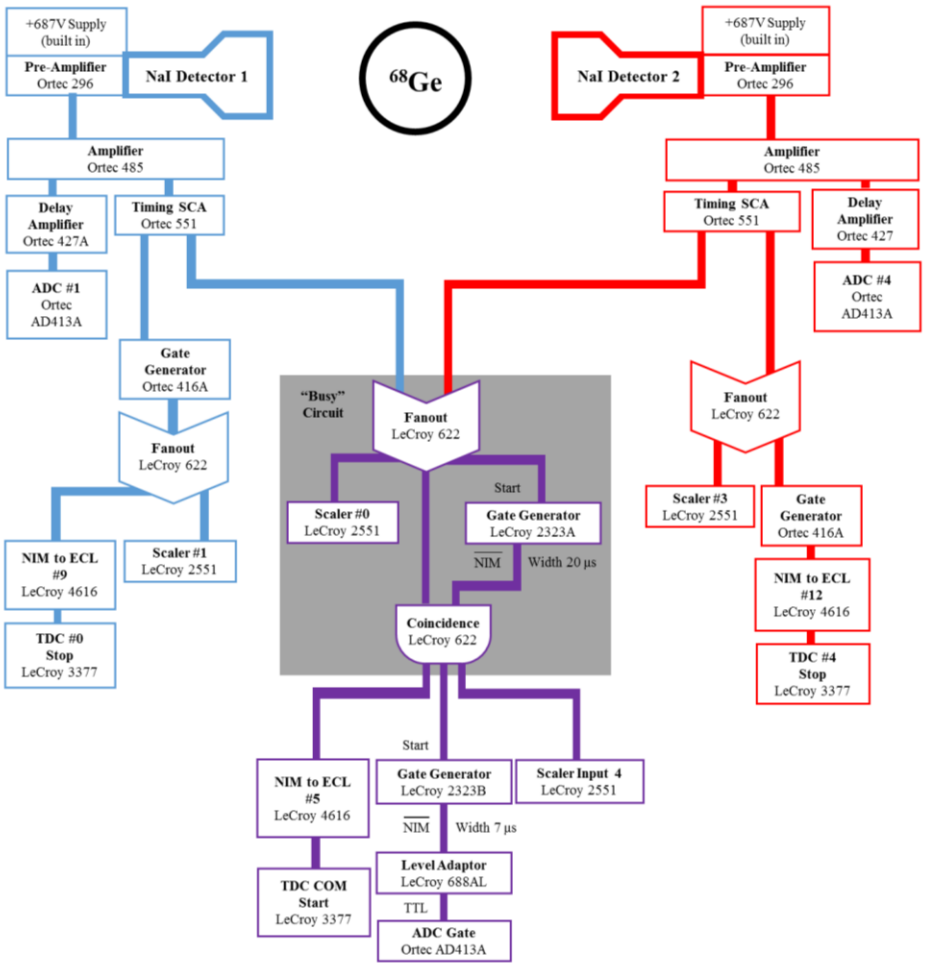

Figure 32. Electronics diagram of Experiment V. Pulses from Detectors I and II were amplified. Pulses that corresponded to gamma rays in the full-peak were selected by TSCAs and the coincidence of those pulses was tested and sent to a CAMAC system for analysis.

When the position of Detectors I and II were varied, the RMS percent difference between GEANT calculation and measurement of absolute full-peak singles efficiency was 11.48% for Detector I and 8.67% for Detector II, as plotted in Figure 33. Absolute full-peak coincidence efficiency had an RMS percent difference of 5.66% as plotted in Figure 34. When the position of the ^{68}Ge was varied, the RMS percent difference between GEANT calculation and measurement of absolute full-peak singles efficiency was 1.73% for Detector I and 4.70% for Detector II as plotted in Figure 35. Absolute full-peak coincidence efficiency had an RMS percent difference of 4.88% as plotted in Figure 36.

These results were encouraging. However, in the Ohio University experiment, gamma rays in the thick graphite disk can Compton scatter before reaching the NaI detectors. Compton scattering occurs when a photon transfers some of its energy to an atomic electron, reducing the energy of the photon and changing its trajectory. Because of this, a pair of 511 keV gamma rays may not be measured in coincidence if either of those photons Compton scatter.

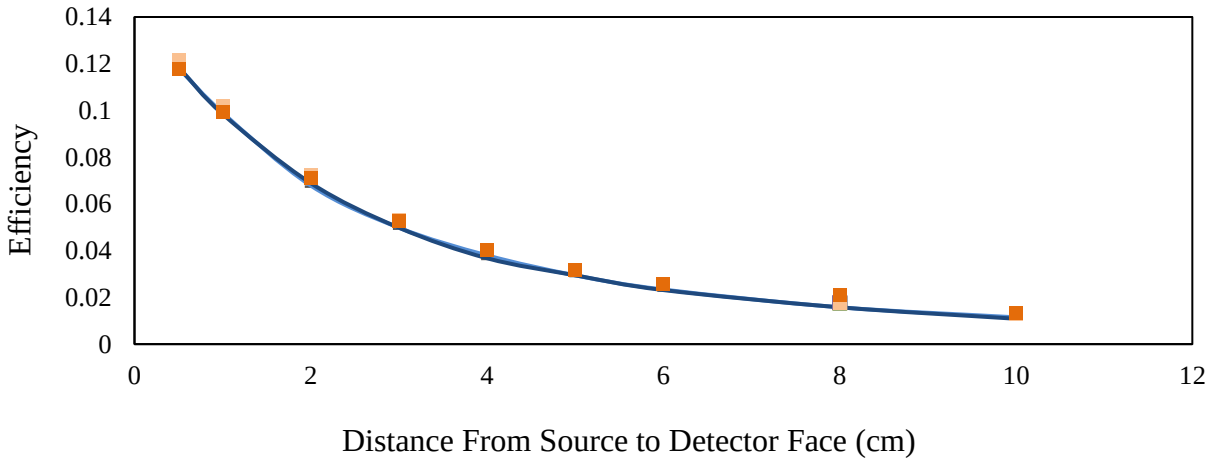

Figure 33. Plot of absolute full-peak singles efficiency for Exp. V as a function of the distance between ^{68}Ge and faces of Detectors I and II including measured singles efficiency for Detector I (light orange points) and Detector II (dark orange points) as well as simulated singles efficiency for Detector I (light blue curve) and Detector II (dark blue curve). RMS percent difference for Detector I was 11.48% and 8.67% for Detector II.

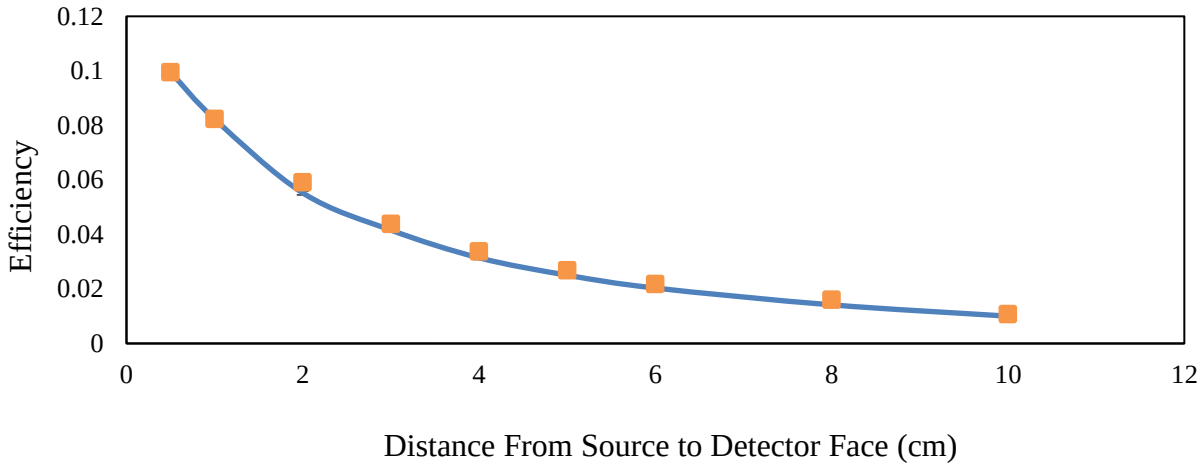

Figure 34. Plot of absolute full-peak coincidence efficiency for Exp. V as a function of the distance between the ^{68}Ge source and the faces of Detectors I and II including measured efficiencies (orange points) and the GEANT simulation (blue curve). RMS percent difference of 5.66%.

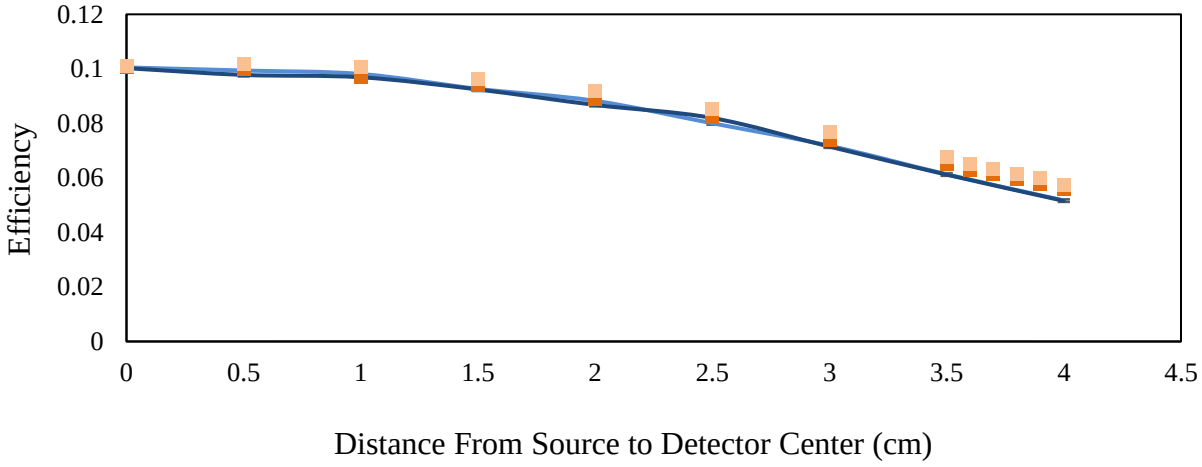

Figure 35. Plot of absolute full-peak singles for Exp. V as a function the distance between the center of the ^{68}Ge disk source and the shared axis of Detectors I and II including measured singles efficiency for Detector I (light orange points) and Detector II (dark orange points) as well as simulated singles efficiency for Detector I (light blue curve) and Detector II (dark blue curve). RMS percent difference for Detector I was 1.73% and 4.70% for Detector II.

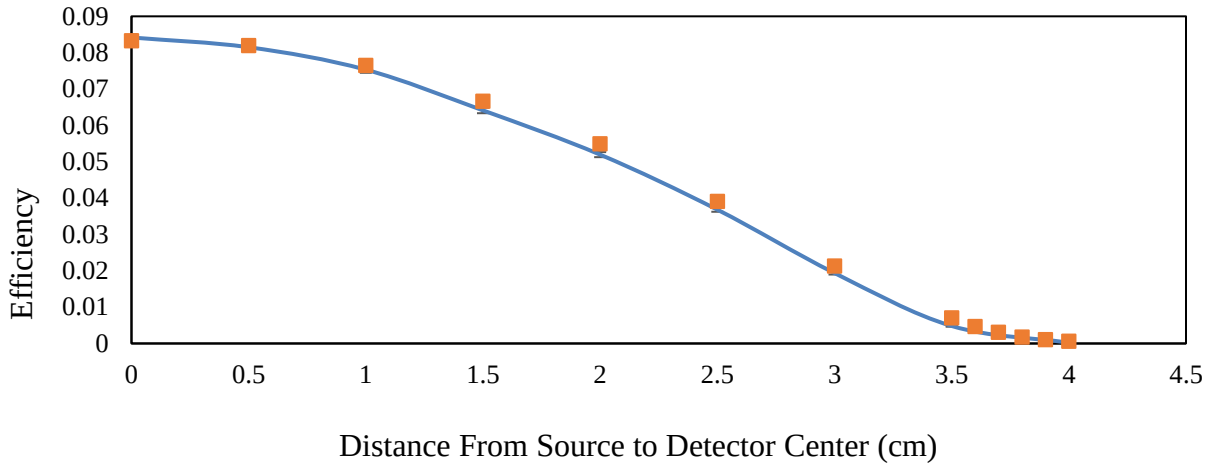

Figure 36. Plot of absolute full-peak coincidence efficiency for Exp. V as a function of the distance between the center of the ^{68}Ge disk source and the shared axis of Detectors I and II including measured efficiencies (orange points) and the GEANT simulation (blue curve). RMS percent difference 4.88%.

3.6 Experiment VI: Measurement of Compton Scattering Effects

Experiment VI tested the ability of the GEANT code to include the effects of Compton scattering by placing the ^{68}Ge source between disks of graphite. This graphite had the same geometry as the disks used in the Ohio University Experiment. Figure 37 is a photograph of the setup for Experiment VI. The electronics for Experiment VI were the same as in Experiment V, as shown in Figure 32.

The ^{68}Ge source was encased in a thin layer of kapton and Mylar. It was taped to the graphite using scotch tape. The thickness of the graphite between the positron source and NaI detectors was varied across several measurements using 2.45 mm thick disks. In the first measurement, 1 disk was placed on either side of the source. In the second, 3 disks were placed on one side of the source and 1 disk on the other side. In the third, 3 disks were placed on either side of the source. The position of the source was varied along a straight line parallel to the plane of symmetry of the NaI detectors. GEANT simulations corresponding to these geometries were created for comparison.

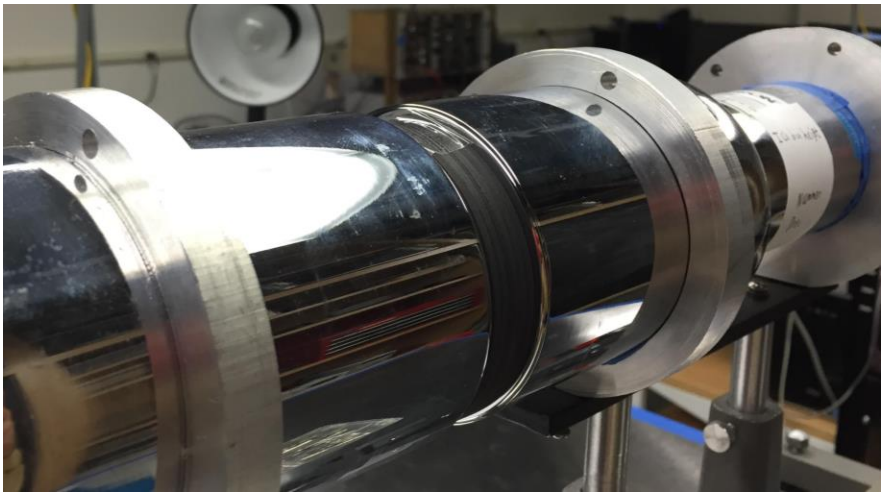

Figure 37. The setup for Exp. VI. A NIST calibrated ^{68}Ge source was placed between graphite disks to test how well GEANT simulated Compton scattering.

The absolute full-peak singles and coincidence efficiencies were calculated and measured with respect to the position of the source. When 2.45 mm of graphite was placed on either side of the ^{68}Ge, the RMS percent difference between GEANT calculation and measurement of absolute full-peak singles efficiency was 1.98% for Detector I and 1.59% for Detector II as plotted in Figure 38. Absolute full-peak coincidence efficiency had an RMS percent difference of 4.46% as plotted in Figure 39. When 2.45 mm of graphite was placed between the source and Detector I and 7.35 mm of graphite was placed between the source and Detector II, the RMS percent difference between GEANT calculation and measurement of absolute full-peak singles efficiency was 2.95% for Detector I and 5.67% for Detector II as plotted in Figure 40. Absolute full-peak coincidence efficiency had an RMS percent difference of 18.38% as plotted in Figure 41. When 7.35 mm of graphite was placed on either side of the source between Detectors I and II, the RMS percent difference between GEANT calculation and measurement of absolute full-peak singles efficiency was 1.21% for Detector I and 0.82% for Detector II as plotted in Figure 42. Absolute full-peak coincidence efficiency had an RMS percent difference of 8.63% as plotted in Figure 43.

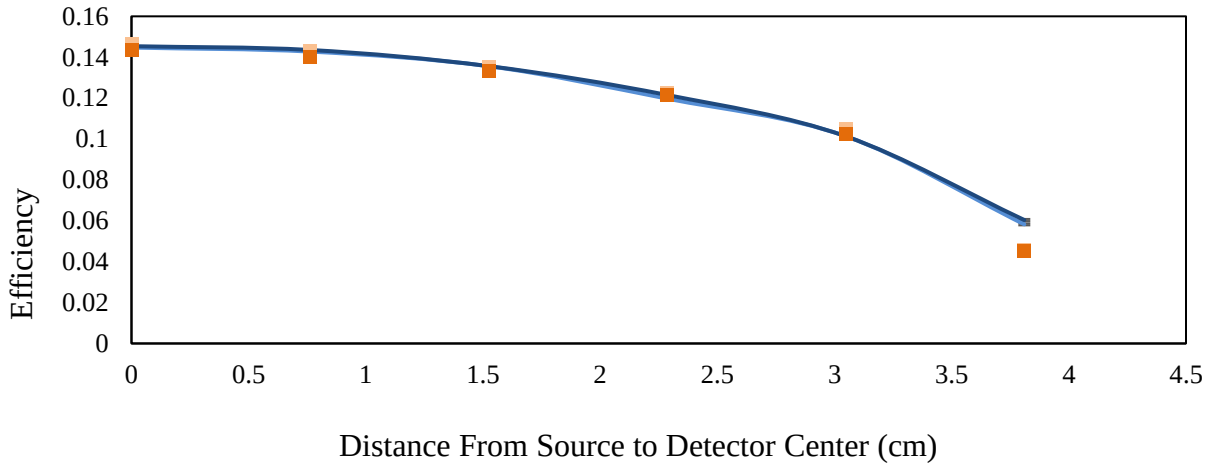

Figure 38. Plot of absolute full-peak singles efficiency for Exp. VI with 2.45 mm of graphite on either side of the ^{68}Ge as a function of the source position from the shared axis of Detectors I and II including measured singles efficiency for Detector I (light orange points) and Detector II (dark orange points) as well as simulated singles efficiency for Detector I (light blue curve) and Detector II (dark blue curve). RMS percent difference for Detector I was 1.98% and 1.59% for Detector II.

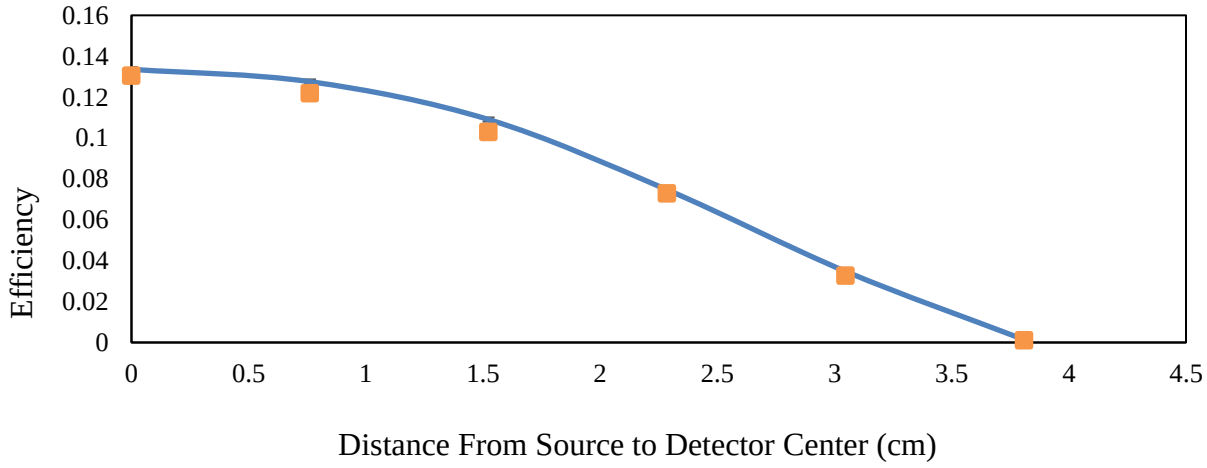

Figure 39. Plot of absolute full-peak coincidence efficiency for Exp. VI with 2.45 mm of graphite on either side of the ^{68}Ge as a function of the source position from the shared axis of Detectors I and II including measured values (orange squares) and the GEANT simulation (blue curve). RMS percent difference of 4.46%.

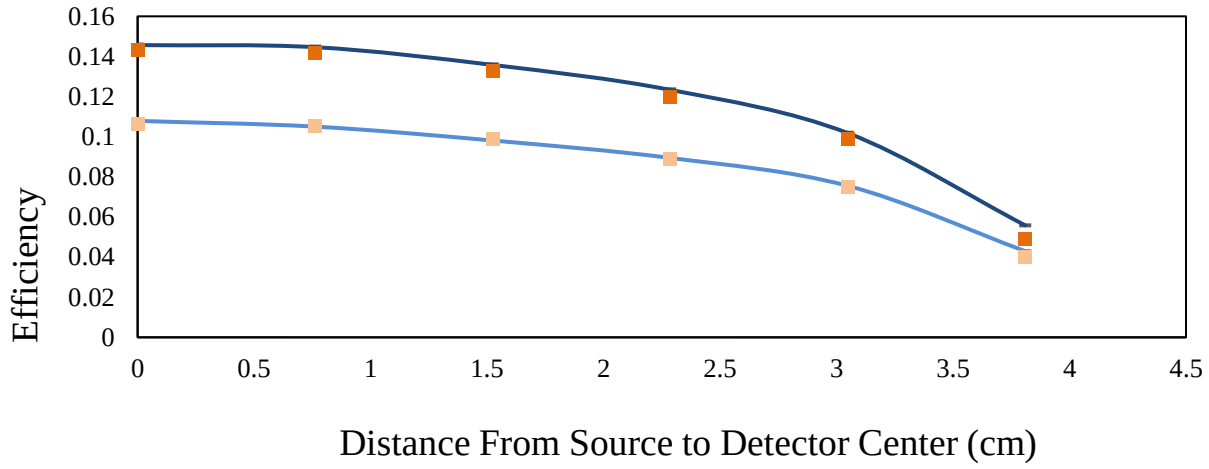

Figure 40. Plot of absolute full-peak singles efficiency for Exp. VI with asymmetric graphite thicknesses of 2.45 mm on Detector I side and 7.35 mm on Detector II side of the ^{68}Ge as a function of the source position from the shared axis of Detectors I and II including measured singles efficiency for Detector I (light orange points) and Detector II (dark orange points) as well as simulated singles efficiency for Detector I (light blue curve) and Detector II (dark blue curve). RMS percent difference for Detector I was 2.95% and 5.67% for Detector II.

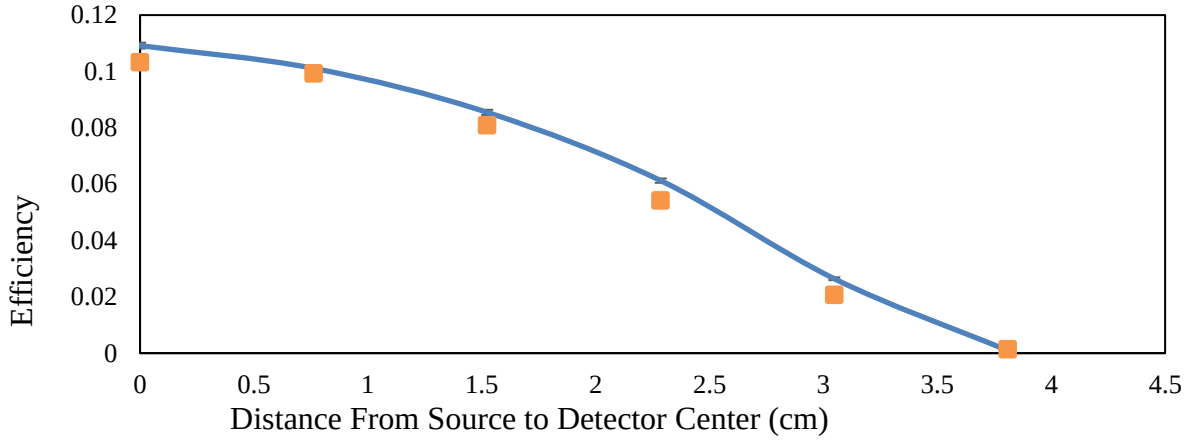

Figure 41. Plot of absolute full-peak coincidence efficiency for Exp. VI with asymmetric graphite thicknesses of 2.45 mm on Detector I side and 7.35 mm on Detector II side of the ^{68}Ge as a function of the source position from the shared axis of Detectors I and II including measured values (orange squares) and the GEANT simulation (blue curve). RMS percent difference of 18.38%

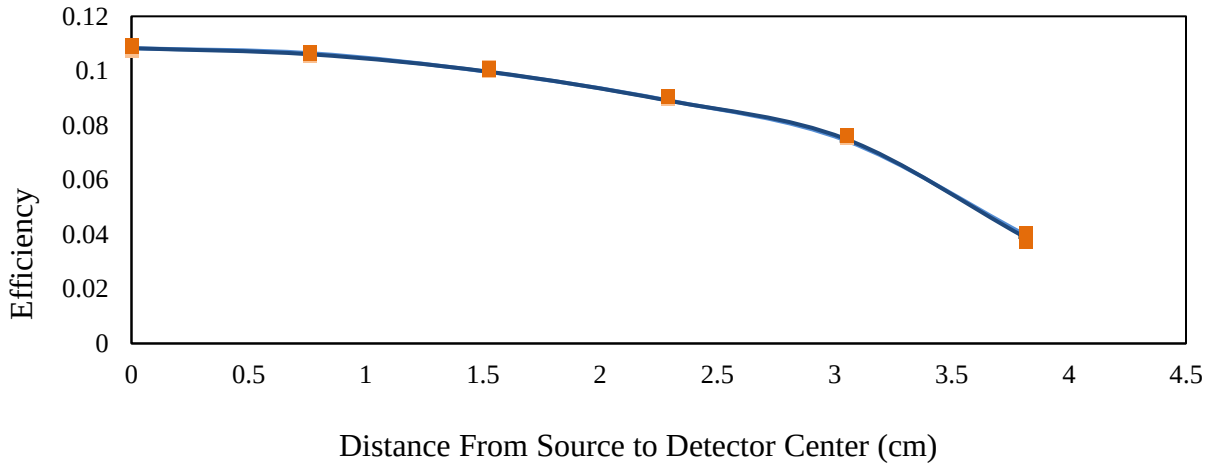

Figure 42. Plot of absolute full-peak singles efficiency for Exp. VI with 7.35 mm of graphite on either side of the ^{68}Ge as a function of the source position from the shared axis of Detectors I and II including measured singles efficiency for Detector I (light orange points) and Detector II (dark orange points) as well as simulated singles efficiency for Detector I (light blue curve) and Detector II (dark blue curve). RMS percent difference for Detector I was 1.21% and 0.82% for Detector II.

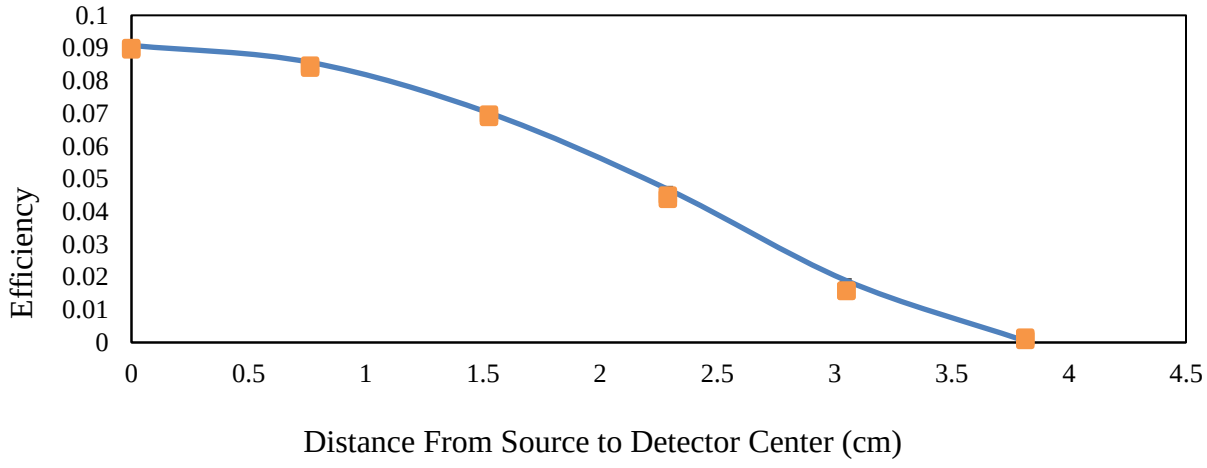

Figure 43. Plot of absolute full-peak coincidence efficiency for Exp. VI with 7.35 mm of graphite on either side of the ^{68}Ge as a function of the source position from the shared axis of Detectors I and II including measured values (orange squares) and the GEANT simulation (blue curve). RMS percent difference of 8.63%.

Chapter 4

RESULTS AND CONCLUSIONS

Once the GEANT simulation was validated by comparing with experimental data, it was used to calculate the coincidence efficiency of the detectors used in measuring the number of ^{11}C present in the plastic and carbon disks used for the Ohio University experiment described in Section 1.2.6. Knowing the number of ^{11}C in the disks allowed for the measurement of the $^{12}C(n, 2n)^{11}C$ cross section to be completed.

4.1 Simulation of the Ohio University Experiment

Using the calibrated GEANT code, efficiencies for both Detectors I and II measuring ^{11}C decay in the carbon and polyethylene disks for the Ohio University Experiment were calculated as shown in Table 2. Using the RMS percent differences in experiments IV through VI, a systematic uncertainty of 5.0% was assigned to the absolute full-peak efficiency calculations.

Table 2. Absolute full-peak efficiencies for the Ohio University Experiment calculated using the GEANT code. These values were used to find the $^{12}C(n, 2n)^{11}C$ cross section.

Target	**Configuration**	**Efficiency**
Graphite	Coincidence	0.0494 ± 0.0025
	Detector I	0.0981 ± 0.0049
	Detector II	0.1049 ± 0.0052
Polyethylene	Coincidence	0.1568 ± 0.0078
	Detector I	0.1655 ± 0.0083
	Detector II	0.1655 ± 0.0083

This simulation included variation in the distribution of ^{11}C in the graphite disk based on an MCNP5 model of the distribution of incident neutrons on the disk. The model showed, relatively independent

of neutron energy, that the density of ^{11}C fell to 75% on the downstream face compared to the upstream face of the graphite disk, and the density fell 5% from the center of the disk to its edge. This resulted in a 6% increase in simulated coincidence efficiency with only a slight increase in singles efficiency for the detector close to the upstream face.

4.2 The $^{12}C(n, 2n)^{11}C$ Cross Section

Using the efficiency values calculated in Table 2, values for the $^{12}C(n, 2n)^{11}C$ cross section were produced with an approximate uncertainty of 5%. Figure 44 is a plot of the preliminary cross section values obtained. These values are recorded in Table 3.

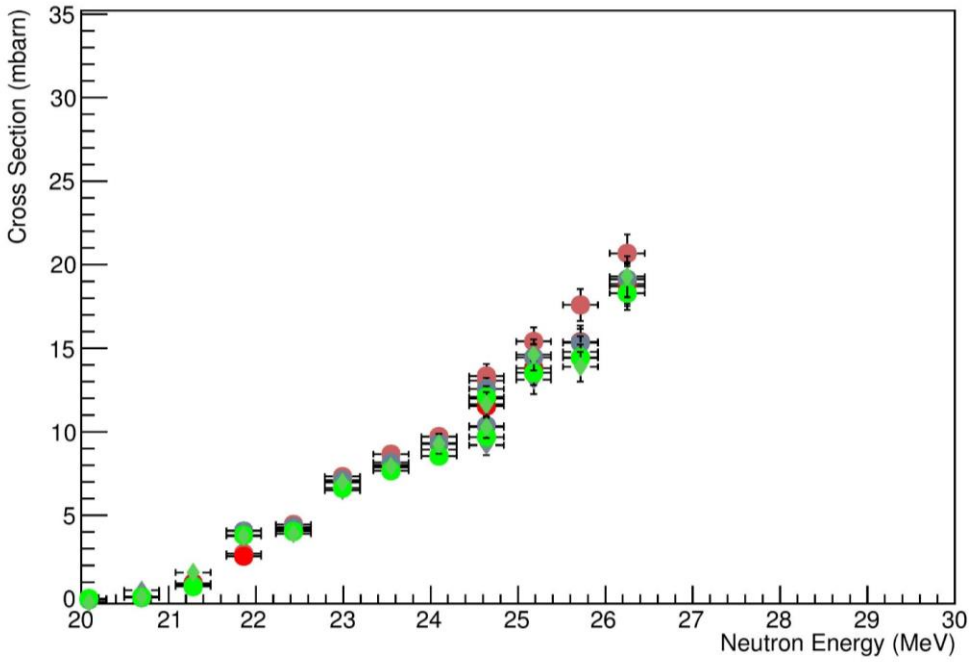

Figure 44. Plot of preliminary $^{12}C(n, 2n)^{11}C$ cross section as a function of incident neutron energy including values as calculated in this experiment using graphite disk decays measured in coincidence (pink circles), polyethylene disk decays measured in coincidence (red circles), graphite disk decays measured by Detector I (grey circles), polyethylene decays measured by Detector I (grey diamonds), graphite disk decays measured by Detector II (green circles), and polyethylene disk decays measured by Detector II (green diamonds).

Table 3. The preliminary $^{12}C(n, 2n)^{11}C$ cross section as a function of incident neutron energy measured by this experiment including values found by graphite and polyethylene disk decay measurements using Detector I, Detector II, and coincidence for both.

Incident Energy (MeV)	Graphite Coincidence (mb)	Graphite Detector I (mb)	Graphite Detector II (mb)	Polyethylene Coincidence (mb)	Polyethylene Detector I (mb)	Polyethylene Detector II (mb)
19.5 ± 0.2	0.00 ± 0.00	0.00 ± 0.00	0.00 ± 0.00	0.00 ± 0.00	0.00 ± 0.00	0.00 ± 0.00
20.1 ± 0.2	0.00 ± 0.00	-0.05 ± 0.01	0.02 ± 0.01	0.00 ± 0.01	-0.04 ± 0.13	-0.21 ± 0.01
20.7 ± 0.2	0.08 ± 0.00	0.08 ± 0.01	0.11 ± 0.01	0.08 ± 0.01	0.51 ± 0.10	0.12 ± 0.01
21.3 ± 0.2	0.83 ± 0.04	0.80 ± 0.04	0.74 ± 0.04	0.93 ± 0.05	0.84 ± 0.09	1.57 ± 0.05
21.9 ± 0.2	2.72 ± 0.14	4.07 ± 0.21	3.82 ± 0.19	2.55 ± 0.13	4.07 ± 0.22	3.74 ± 0.13
22.4 ± 0.2	4.47 ± 0.23	4.31 ± 0.22	4.05 ± 0.20	4.08 ± 0.21	4.20 ± 0.23	3.89 ± 0.21
23.0 ± 0.2	7.34 ± 0.37	7.11 ± 0.36	6.64 ± 0.34	7.01 ± 0.36	6.47 ± 0.37	6.96 ± 0.36
23.5 ± 0.2	8.68 ± 0.44	8.18 ± 0.41	7.69 ± 0.39	7.99 ± 0.41	7.83 ± 0.40	7.88 ± 0.41
24.1 ± 0.2	9.73 ± 0.49	9.34 ± 0.47	8.57 ± 0.43	9.26 ± 0.47	8.91 ± 0.46	9.25 ± 0.47
24.6 ± 0.2	13.37 ± 0.67	12.59 ± 0.63	12.10 ± 0.61	11.95 ± 0.61	11.54 ± 0.59	11.61 ± 0.61
24.6 ± 0.2	13.10 ± 0.66	10.38 ± 0.52	9.72 ± 0.49	11.51 ± 0.59	9.17 ± 0.47	10.25 ± 0.59
25.2 ± 0.2	15.44 ± 0.78	14.49 ± 0.73	13.56 ± 0.69	13.75 ± 0.70	13.07 ± 0.67	14.56 ± 0.70
25.7 ± 0.2	17.63 ± 0.89	15.36 ± 0.78	14.46 ± 0.73	15.33 ± 0.78	14.73 ± 0.76	13.85 ± 0.78
26.3 ± 0.2	20.73 ± 1.05	19.17 ± 0.97	18.34 ± 0.93	18.79 ± 0.96	18.65 ± 0.96	19.23 ± 0.96

4.3 Comparison to Previous Measurements

Plotting the preliminary $^{12}C(n, 2n)^{11}C$ cross section measured in this experiment as in Figure 45 show that the values measured by this experiment tend to follow the values calculated by P.J. Dimbylow in Ref [12]. These values were calculated using a nuclear optical model in which the ^{12}C nucleus was simulated as a fermi gas composed of neutrons and protons.

Further measurements of the cross section at higher energies by the method used in this experiment would require an accelerator able to deliver deuterons to a tritide target at energies above 13 MeV. However, for the purpose of developing a diagnostic to measure the areal density of ICF, this measurement is sufficient as the flux of tertiary neutrons goes drops off quickly above 27 MeV.

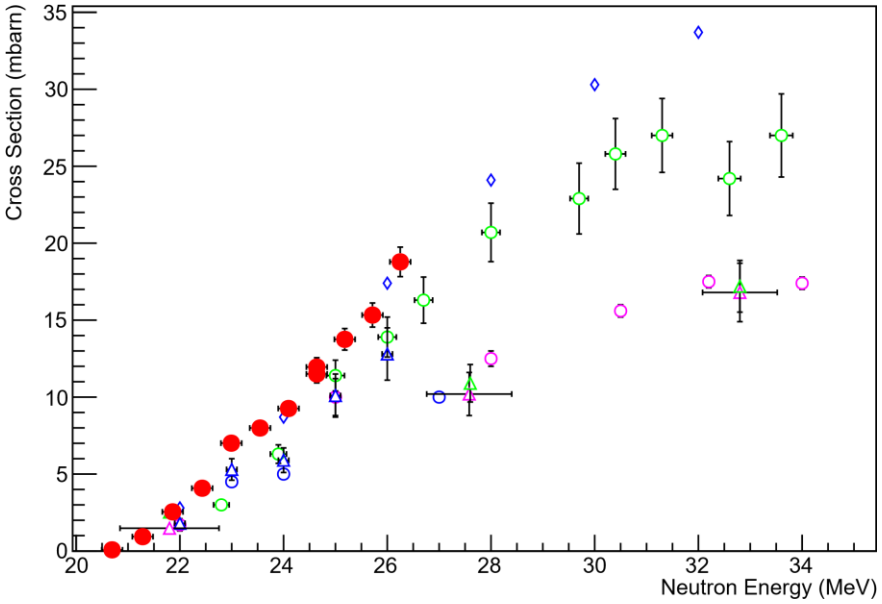

Figure 45. Plot of all $^{12}C(n, 2n)^{11}C$ cross section values as a function of incident neutron energy including values measured in this experiment using polyethylene disk decays measured in coincidence (red circles), and published cross-sections for the $^{12}C(n, 2n)^{11}C$ reaction from Brolley et al. [6] (blue circles), Brill et al. [7] (pink circles), Anders et al. [8] (green circles), Welch et al. [9] (blue triangles), Soewarsono et al. [10] (pink triangles), Uno et al. [11] (green triangles), and Dimbylow [12] (blue diamonds). The measurement for this experiment tends to follow the values measured by Dimbylow.

Acknowledgement

I would like to thank Cody Parker for operating the accelerator; Dr. Ryan Fitzgerald for help acquiring calibrated sources and developing the GEANT code; Garrett Hartshaw, Andrew Evans, Keith Mann, Tyler Reynolds, Ian Love, August Gula, Laurel Vincett, Angela Simone, Lee Gabler, Michael Krieger, Mollie Bienstock, Collin Stillman, Drew Ellison, and Holly Desmitt for assistance performing the experiment; Dr. Brandon Hoffman for reading; Dr. Mark Yuly for being my guide and mentor in accomplishing this measurement. This research is funded in part by the University of Rochester Laboratory for Laser Energetics through a grant from the Department of Energy.

Appendix

CODE LISTING

A.1 Simple Monte-Carlo

This Monte-Carlo code was written by Dr. Mark Yuly to calculate absolute total efficiency for NaI detectors in Experiments I and II.

```
/*
Calculate total efficiency of single 3 x 3 NaI crystal
Based on paper by Yalcin et al, Appl Radiation and Isotopes 65, 1179 (2007)
ROOT macro
Input parameters:
s_dist = perpendicular distance from source face to NaI det face(cm)
s_thick = thickness of source (cm)
s_radius = source radius (cm)
s_r_pos = radial location of source (cm)
Note: phi position of source is assumed to be 0 deg.
*/

struct str_cyl {
  double enter_x, enter_y, enter_z;
  double exit_x, exit_y, exit_z;
  double DS;
};

struct eff {
  double efficiency, efficiency1, efficiency2;
};

eff montecarlo_double(double s_dist, double s_thick, double s_radius, double
s_r_pos){

  Double_t worldRadius=60;
  int i_plot = 1;
  int N_plot_coinc = 10000;  // number gammas to plot for gamma in both detect
                             // -1 to turn off
  int N = 10000;             // number of photons to track (1000000?)

  TRandom3 rnd;                 // random number generator
  double ra;                    // distance from center
  double s_x, s_y, s_z, s_z2;   // x y and z position of source point
  double phiprime;              // phi location of source point
  double phi, phi2;             // phi direction for gamma
```

```
double costheta;              // theta direction for gamma
double S=0, S1=0, S2=0;
double TS=0, TS1=0, TS2=0;

str_cyl NaI1, Air1, Al1, Gr1;
str_cyl NaI2, Air2, Al2, Gr2;
eff return_eff;

// Constants

double mu_NaI = 0.342;     // cm^-1, att coef for NaI at 0.511 MeV from XCOM
double rd_NaI = 3.81;      // cm, radius of NaI crystal (1.5 inch)
double hd_NaI = 7.62;      // cm, length of NaI crystal (3 inch)

double mu_Si_case = 0.663;
    // cm^-1, att coef for assumed Fe case of Si det at 0.511 MeV from XCOM
double rd_Si_case_i = 0.28;
    // cm, inside radius of Si det case (0.22 inch diam)
double rd_Si_case_o = 0.833;
    // cm, outside radius of Si det case  (0.656 inch diam)
double hd_Si_case = 0.2;
    // cm, length of Si det case

double mu_Air = 0.000112;   // cm^-1, att coef for Air at 0.511 MeV from XCOM
double rd_Air = 3.81;       // cm, radius of air layer

double mu_Al = 0.228;  // cm^-1, att coef for Al cover at 0.511 MeV from XCOM
double rd_Al = 3.81;   // cm, radius of aluminum cover (1.5 inch)
double hd_Al = 0.051;  // cm, thickness of aluminum cover (0.02 inch)

double mu_g = 0.186;   // cm^-1, att coef for graphite at 0.511 MeV
double rd_g = 3.81;    // cm, radius of graphite (1.5 inch)
double hd_g = 0.89;    // cm, thickness of graphite

double mu_p = 0.0986;  // cm^-1, att coef for polyeth at 0.511 MeV (XCOM)
double rd_p = 1.27;    // cm, radius of polyethylene
double hd_p = 0.164;   // cm, thickness of polyethylene

double pi = 3.141593;  // pi

gRandom->SetSeed();

// Set up GL viewer, sphere volume
if (N_plot_coinc>0 ){
  TGeoTranslation * trans;
  TGeoManager * geom = new TGeoManager("LODTest", "GL viewer LOD test");
  geom->SetNsegments(4); //Set number of segments for approx circle, keep low
  TGeoMaterial *matEmptySpace = new TGeoMaterial("EmptySpace", 0, 0, 0);
  TGeoMaterial *matSolid = new TGeoMaterial("Solid", .938, 1., 10000.);

  TGeoMedium *medEmptySpace = new TGeoMedium("Empty", 1, matEmptySpace);
```

```
  TGeoMedium *medSolid  = new TGeoMedium("Solid", 1, matSolid);

  TGeoVolume*top = geom->MakeBox("WORLD", medEmptySpace, worldRadius,
    worldRadius, worldRadius);
  geom->SetTopVolume(top);

  TGeoVolume * volume_red = new TGeoVolume;
  volume_red = geom->MakeSphere("Sphere1", medSolid, 0., 0.1);
  volume_red->SetLineColor(kRed);

  TGeoVolume * volume_blue = new TGeoVolume;
  volume_blue = geom->MakeSphere("Sphere2", medSolid, 0., 0.05);
  volume_blue->SetLineColor(kBlue);

  TGeoVolume * volume_ltblue = new TGeoVolume;
  volume_ltblue = geom->MakeSphere("Sphere3", medSolid, 0., 0.05);
  volume_ltblue->SetLineColor(kBlue-9);

  TGeoVolume * volume_green = new TGeoVolume;
  volume_green = geom->MakeSphere("Sphere4", medSolid, 0., 0.05);
  volume_green->SetLineColor(kGreen+3);

  TGeoVolume * volume_ltgreen = new TGeoVolume;
  volume_ltgreen = geom->MakeSphere("Sphere5", medSolid, 0., 0.1);
  volume_ltgreen->SetLineColor(kGreen-6);
}

// Loop of tracks -- rnd.Rndm() gives random number 0 to 1
for (int i=0; i<N; i++){
  // show count by 1000s
  if ( (int)(i/1000) *1000 == i) printf("i = %d\n",i);

  // loop until source point is inside source radius
  do{
    s_x = s_r_pos + (rnd.Rndm()-0.5)*2*s_radius;
    s_y = (rnd.Rndm()-0.5)*2*s_radius;
    s_z = -rnd.Rndm()*s_thick;
  } while ( (s_x-s_r_pos)**2 + s_y**2 > s_radius**2 );

  //axial polar coordinate of source
  if (s_y>=0 && s_x>=0) phiprime = atan(s_y/s_x);
  if (s_y<0 && s_x<0) phiprime = pi + atan(s_y/s_x); // take care!
  if (s_y<0 && s_x>=0) phiprime = atan(s_y/s_x);
  if (s_y>=0 && s_x<0) phiprime = pi + atan(s_y/s_x);

  ra = sqrt(s_x**2 + s_y**2);  // radial polar coordinate of source point

  phi = 2*pi*rnd.Rndm();    // generate random phi direction for gamma
  costheta = rnd.Rndm();    // generate random theta direction for gamma
```

```
//*************************************************************************
// FIRST DO GAMMA ONE DIRECTION
//*************************************************************************

// Do graphite
Gr1 = a_cyl(s_z, s_z, ra, phiprime, costheta, phi, mu_g, rd_g, -s_z);
// gamma attenuation in graphite

// Do Al on front of NaI
Al1 = a_cyl(s_dist, s_z, ra, phiprime, costheta, phi, mu_Al, rd_Al, hd_Al);
// gamma attenuation in Al sheild in front of  NaI detector

// Do NaI detector
NaI1 = a_cyl(s_dist,s_z,ra,phiprime,costheta,phi,mu_NaI,rd_NaI,hd_NaI);
// gamma attenuation in NaI detector

//*************************************************************************
// NOW DO GAMMA AT 180 DEG
//*************************************************************************

phi2 = phi + pi;
s_z2 = -(s_thick + s_z);

// Do Graphite
Gr2 = a_cyl(s_z2, s_z2, ra, phiprime, costheta, phi2, mu_g, rd_g, -s_z2);
// gamma attenuation in graphite

// Do Al on front of NaI
Al2 = a_cyl(s_dist,s_z2,ra,phiprime,costheta,phi2,mu_Al,rd_Al,hd_Al);
// gamma attenuation in Al shield in front of NaI detector

// Do NaI detector
NaI2 = a_cyl(s_dist,s_z2,ra,phiprime,costheta,phi2,mu_NaI,rd_NaI,hd_NaI);
// gamma attenuation in NaI detector

if (i_plot<N_plot_coinc && NaI2.DS != 1&& NaI1.DS != 1){
  //printf("source i x, y, z %d %f %f  %f\n", i, s_x, s_y, s_z);
  trans = new TGeoTranslation(s_x, s_y, s_z);
  top->AddNode(volume_red, 10*i, trans);

  //printf("Gr1 enter i x, y, z %d %f %f %f\n", i,
  //Gr1.enter_x, Gr1.enter_y, Gr1.enter_z);
  //trans = new TGeoTranslation(Gr1.enter_x, Gr1.enter_y, Gr1.enter_z);
  //top->AddNode(volume_blue,10*i+1, trans);

  //printf("Gr1 exit i x, y, z %d %f %f %f\n", i,
  //Gr1.exit_x, Gr1.exit_y, Gr1.exit_z);
  //trans = new TGeoTranslation(Gr1.exit_x, Gr1.exit_y, Gr1.exit_z);
  //top->AddNode(volume_ltblue, 10*i+2, trans);
```

```
  //printf("Gr2 enter i x, y, z %d %f %f %f\n", i,
  //Gr2.enter_x, Gr2.enter_y, -s_thick-Gr2.enter_z);
  //trans= new TGeoTranslation(Gr2.enter_x, Gr2.enter_y,
  //-s_thick-Gr2.enter_z);
  //top->AddNode(volume_blue,10*i+3, trans);

  //printf("Gr2 exit i x, y, z %d %f %f %f\n", i,
  //Gr2.exit_x, Gr2.exit_y, -s_thick-Gr2.exit_z);
  //trans = new TGeoTranslation(Gr2.exit_x, Gr2.exit_y,
  //-s_thick-Gr2.exit_z);
  //top->AddNode(volume_ltblue, 10*i+4, trans);

  //printf("NaI1 enter i x, y, z %d %f %f  %f\n", i,
  //NaI1.enter_x, NaI1.enter_y, NaI1.enter_z);
  trans = new TGeoTranslation(NaI1.enter_x, NaI1.enter_y, NaI1.enter_z);
  top->AddNode(volume_green,10*i+5, trans);

  //printf("NaI1 exit i x, y, z %d %f %f %f\n", i,
  //NaI1.exit_x, NaI1.exit_y, NaI1.exit_z);
  trans = new TGeoTranslation(NaI1.exit_x, NaI1.exit_y, NaI1.exit_z);
  top->AddNode(volume_ltgreen, 10*i+6, trans);

  //printf("NaI2 enter i x, y, z %d %f %f %f\n", i,
  NaI2.enter_x, NaI2.enter_y, -s_thick-NaI2.enter_z);
  trans= new TGeoTranslation(NaI2.enter_x, NaI2.enter_y,
    -s_thick-NaI2.enter_z);
  top->AddNode(volume_green,10*i+7, trans);

  //printf("NaI2 exit i x, y, z %d %f %f %f\n", i,
  //NaI2.exit_x, NaI2.exit_y, -s_thick-NaI2.exit_z);
  trans = new TGeoTranslation(NaI2.exit_x, NaI2.exit_y,
    -s_thick-NaI2.exit_z);
  top->AddNode(volume_ltgreen, 10*i+8, trans);

  i_plot++;
}

//*********************************************************************
// NOW DO PROBABILITY SUMS
//*********************************************************************

// remember, DS is probability that gamma does not interact
// if either NaI.DS = 1 (i.e. it missed) then S = 0

S = Gr1.DS*Al1.DS*Gr2.DS*Al2.DS*(1 - NaI1.DS)*(1 - NaI2.DS);
// prob gamma passes through det case and interacts in NaI

S1 = Gr1.DS*Al1.DS*(1 - NaI1.DS); // singles det 1
S2 = Gr2.DS*Al2.DS*(1 - NaI2.DS); // singles det 2
//if (S!=0.) printf("s s1 s2 %f %f %f\n",S,S1,S2);
```

```
    TS = TS + S;
    TS1 = TS1 + S1;
    TS2 = TS2 + S2;
  }

  return_eff.efficiency = TS/(N);
  return_eff.efficiency1 = TS1/(2.0*N);
  return_eff.efficiency2 = TS2/(2.0*N);

  if (N_plot_coinc>0 ){
    geom->CloseGeometry();
    top->Draw("ogl");
  }

  printf("efficiency: %f %f %f\n", return_eff.efficiency,
  return_eff.efficiency1, return_eff.efficiency2);
  return  return_eff;  // total efficiency
}

str_cyl a_cyl(double s_dist, double s_z, double ra, double phiprime, double
costheta, double phi, double mu, double rd, double hd) {

  /*
  Calculate probabily of gamma not being absorbed in cylinder
  s_dist = distance from face of source to face of cylinder (cm)
  s_z = distance from face of source to source point (cm) (negative)
  ra = radial coordinate of source point (cm)
  phiprime = axial coordinate of source point (rad)
  costheta = cosine of gamma direction angle from z axis (rad)
  phi = polar direction angle (from x axis) of gamma ray (rad)
  mu = gamma attenuation coef (cm^-1)
  rd = radius of cylinder (cm)
  hd = height of cylinder (cm)
  */

  str_cyl return_value;
  double s;
  double sintheta;    // theta direction for gamma
  double d;           // distance from source point to face of cyl
  double aprime;
  double alpha1, alpha2;
  double delta=0;

  // distance from source point to front of cylinder
  d = s_dist - s_z;

  // distance from source point to cyl wall in direction of gamma in xy plane
  aprime = ra*cos(phi) + sqrt( (ra*cos(phi))**2 - (ra**2 - rd**2) );
```

```
  // theta must be less than alpha2 to enter detector
  alpha2 = atan( aprime/d);
  //printf("%f%f%f%f%f%f%f\n", costheta, alpha2, d, phi, phiprime, s_dist, hd);
  if (costheta > cos(alpha2))   // enters detector
  {
    // determine front face entrance coordinates
    sintheta = sqrt(1-costheta**2);
    s = d*sintheta/costheta;   // tan(theta)
    return_value.enter_x = ra*cos(phiprime) - s*cos(phi-phiprime);
    return_value.enter_y = ra*sin(phiprime) + s*sin(phi-phiprime);
    return_value.enter_z = s_dist;

    // theta must be less than alpha1 to exit back face of cyliner
    alpha1 = atan( aprime/ (d+hd) );

    if (costheta<cos(alpha1))   // exit side
    {
      delta = (aprime/sintheta) - (d/costheta);

      // calculate exit point side
      s = aprime;
      return_value.exit_x = ra*cos(phiprime) - s*cos(phi-phiprime);
      return_value.exit_y = ra*sin(phiprime) + s*sin(phi-phiprime);
      return_value.exit_z = aprime*costheta/sintheta+s_z;
    }

    else       // exit back
    {
      delta = hd/costheta;

      // calculate exit point back
      s = (d+hd)*sintheta/costheta;
      return_value.exit_x = ra*cos(phiprime) - s*cos(phi-phiprime);
      return_value.exit_y = ra*sin(phiprime) + s*sin(phi-phiprime);
      return_value.exit_z = s_dist+hd;
    }

    return_value.DS =  exp(-mu*delta);
  }
  else return_value.DS =  1.; // did not enter detector, all gammas transmitted

  return(return_value);
}

str_cyl a_donut(double s_dist, double s_z, double ra, double phiprime, double
costheta, double phi, double mu, double rdi, double rdo, double hd) {

  /*
  Calculate probability of gamma not being absorbed in a donut shape
  Do this using two cylinders...
  s_dist = distance from face of source to face of donut (cm)
```

```
  s_z = distance from face of source to source point (cm) (negative)
  ra = radial coordinate of source point (cm)
  phiprime = axial coordinate of source point (rad)
  costheta = cosine of gamma direction angle from z axis (rad)
  phi = polar direction angle (from x axis) of gamma ray (rad)
  mu = gamma attenuation coef (cm^-1)
  rdi = inside radius of donut (cm)
  rdo = outside radius of donut (cm)
  hd = height of donut (cm)
  */

  str_cyl return_value, c_i, c_o;

  // first determine if gamma hits inner cylinder
  c_i = a_cyl(s_dist, s_z, ra, phiprime, costheta, phi, mu, rdi, hd);
  c_o = a_cyl(s_dist, s_z, ra, phiprime, costheta, phi, mu, rdo, hd);
  return_value = c_o;

  if (c_i.DS == 1.) {
    // Missed the inner cylinder face, so just use outer.
    // This does not return surface hits for the case where the gamma passes
    // through the inner cylinder.  Does attenuation correctly.

    return_value.DS = c_o.DS/c_i.DS;
  }

  else {
    // Hit the inner cylinder face, so need to remove the inner part...
    // Enters the donut where it exits the inner cylinder

    return_value.enter_x = c_i.exit_x;
    return_value.enter_y = c_i.exit_y;
    return_value.enter_z = c_i.exit_z;
    return_value.DS = c_o.DS/c_i.DS;
  }

  return(return_value);
}

double PtoT_ratio(double d) {
  // Calculate the peak-to-total ratio for a given distance d (cm)
  return(-0.0032*d + 0.597);
}

int scan_d(double s_thick, double s_radius, double s_r_pos, double d0, double
d1, int nsteps){
  // Efficiency as function of distance for a disc source at center
  // s_thick = thickness of source (cm)
  // s_radius = source radius (cm)
  // s_r_pos = radial location of source (cm)
  // rs = radius of source (cm)
```

```
  // d0, d1 = starting and ending distances
  // nsteps = number of steps

  double dd=0;
  eff e;

  ofstream myfile;
  myfile.open ("output_d.txt");

  for (int i=0; i<nsteps; i++){
    dd = d0 + (d1-d0)/(nsteps-1) * i;
    e = montecarlo_double(dd, s_thick, s_radius, s_r_pos);
    myfile << dd <<",  "<<e.efficiency<<",
      "<<e.efficiency*PtoT_ratio(dd)**2<<", "<<e.efficiency1<<",
      "<<e.efficiency1*PtoT_ratio(dd)<<", "<<e.efficiency2<<",
      "<<e.efficiency2*PtoT_ratio(dd)<<endl;
  }

  myfile.close();
  return 1;
}

int scan_r(double s_dist, double s_thick, double s_radius, double r0, double
r1, int nsteps, double thick){

  double dd=0;
  double efficiency;

  ofstream myfile;
  myfile.open ("output_r.txt");

  for (int i=0; i<nsteps; i++){
    dd = r0 + (r1-r0)/(nsteps-1) * i;
    efficiency = montecarlo_single(s_dist, s_thick, s_radius, dd);
    myfile << dd <<",  "<<efficiency<<", "<<efficiency*PtoT_ratio(dd)<<endl;
    cout << dd <<",  "<<efficiency<<", "<<efficiency*PtoT_ratio(dd)<<endl;
    }

  myfile.close();
  return 1;
}
```

A.2 Apparatus simulated in GEANT Monte-Carlo

A.2.1 Materials and Volumes Created in "LTAC1DetectorConstruction.cc"

This code first calls instances of elements in the GEANT libraries then uses them to create compound materials for later use. It creates a volume in which the apparatuses can be simulated before those

apparatuses, including the NaI detectors, scintillation detector, and carbon disks are defined as shown in A.2.2, A.2.3, and A.2.4, uniquely for each experiment.

```
G4VPhysicalVolume* LTAC1DetectorConstruction::Construct()
{
  G4double a;                              // atomic mass
  G4double z;                              // atomic number
  G4double density;                        // density of a substance
  G4double fractionmass;                   // fraction by mass of a mixture
  G4int ncomponents;                       // number of components for compound

  G4NistManager* manager = G4NistManager::Instance();        // NIST substances

  G4Element* elC = manager->FindOrBuildElement("C");
  G4Element* elN = manager->FindOrBuildElement("N");
  G4Element* elNa = manager->FindOrBuildElement("Na");
  G4Element* elI = manager->FindOrBuildElement("I");
  G4Element* elTl = manager->FindOrBuildElement("Tl");
  G4Element* elAl = manager->FindOrBuildElement("Al");
  G4Element* elH = manager->FindOrBuildElement("H");
  G4Element* elBa = manager->FindOrBuildElement("Ba");
  G4Element* elO = manager->FindOrBuildElement("O");

  // Aluminum for NaI detector shells
  G4Material* Al = new G4Material("Aluminum", z = 13., a = 26.98*g/mole,
     density= 2.7*g/cm3);

  // Nitrogen gas fills the simulated room
  G4Material *N2 = new G4Material("N2", density = 1.2*mg/cm3, ncomponents = 1);
  N2->AddElement(elN, 2);

  // Graphite for carbon disk in Ohio C and Experiment V
  G4Material *Graphite = new G4Material("Graphite", density = 1.8*g/cm3,
     ncomponents = 1);
  Graphite->AddElement(elC, 1);

  G4Material *Copper = new G4Material("Copper", density = 8.96*g/cm3,
     ncomponents = 1 );
  Copper->AddElement(elC, 1);

  G4Material *Mylar = new G4Material("Mylar", density = 0.999*g/cm3,
     ncomponents = 4 );
  Mylar->AddElement(elC, 10);
  Mylar->AddElement(elH, 8);
  Mylar->AddElement(elO, 4);
  Mylar->AddElement(elAl, 3);

  G4Material *Kapton = new G4Material("Kapton", density = 1.42*g/cm3,
     ncomponents = 4);
```

```
  Kapton->AddElement(elH, 5);
  Kapton->AddElement(elC, 11);
  Kapton->AddElement(elN, 1);
  Kapton->AddElement(elO, 3);

  // Layer of Barium Oxide around NaI crystal
  G4Material* BaO = new G4Material("BaO", density = 3.0*g/cm3, ncomponents =2);
  BaO->AddElement(elBa, 1);
  BaO->AddElement(elO, 1);

  // Polyvinyltoluene for Experiment IV
  G4Material *Scintillator = new G4Material("Scintillator",
     density = 1.032*g/cm3, ncomponents = 2);
  Scintillator->AddElement(elC, 27);
  Scintillator->AddElement(elH, 30);

  G4Material* NaI = new G4Material("NaI", density = 3.67*g/cm3,
     ncomponents = 2);
  NaI->AddElement(elNa,1);
  NaI->AddElement(elI,1);

// DEFINE NaI(Tl) ------------------//

  G4Material* TlMetal = new G4Material("TlMetal",
     density = 12.*g/cm3, ncomponents = 1);
  TlMetal->AddElement(elTl,1.);

  G4Material* NaI_Tl = new G4Material("NaI_Tl",
     density = 3.67*g/cm3, ncomponents = 2);
  NaI_Tl->AddMaterial(NaI,0.999);
  NaI_Tl->AddMaterial(TlMetal,0.001);

// DEFINE Volumes, starting with room box, in which detectors sit Geometry
// (Box, Tubs...), which gets associated with a, Logical volume, in which
// material is specified, and which gets associated with a, Physical Volume,
// which gets placed in a parent volume (hall is its own volume).

  x_pos = .10*m;
  y_pos = .10*m;
  z_pos = .25*m;
  G4Box* Room_box = new G4Box( "Room_box", x_pos, y_pos, z_pos);
  Room_log = new G4LogicalVolume(Room_box, N2, "Room_log",
     0, 0, 0); // Fill with N2 gas
  Room_phys = new G4PVPlacement(0, G4ThreeVector(), Room_log,
     "Room", 0, false, 0);
```

These materials are then used to simulate the apparatuses for each experiment.

```
;}
```

A.2.2 Construction of Scintillator detector in "LTAC1DetectorConstruction.cc"

```
  //---------------BEGIN--- Scintillator Source ----------------------//

  inner_radius = GetSourceInnerRadius();
  outer_radius = source_radius;
  half_height = source_half_height;
  G4Tubs* Source = new G4Tubs("Source", inner_radius, outer_radius,
     half_height, 0.0, 360.*deg);
  Source_log = new G4LogicalVolume(Source,Scintillator, "Source_log", 0, 0, 0);
  x_pos = source_x_offset;
  y_pos = source_y_offset;
  z_pos = source_z_offset;
  Source_phys = new G4PVPlacement(0, G4ThreeVector(x_pos, y_pos, z_pos),
  Source_log, "Source", Room_log, false, 0);
  G4VisAttributes Source_Att(G4Color::Yellow());
  Source_Att.SetForceWireframe(false);
  Source_Att.SetForceSolid(true);
  Source_Att.SetForceAuxEdgeVisible(true);
  Source_Att.SetVisibility(true);
  Source_log -> SetVisAttributes (Source_Att);

//---------------END--- Scintillator Source ----------------------//
```

A.2.3 Construction of Copper Disks in "LTAC1DetectorConstruction.cc"

```
LTAC1DetectorConstruction::LTAC1DetectorConstruction()
 :  Room_log(0), Room_phys(0), NaI1_log(), NaI2_log(), NaI1_phys(), NaI2_phys()
{

  SetMaterialName("Copper");

  //Source Center Position
  SetSourceXoffset(0.0*cm);
  SetSourceYoffset(0.0*cm);
  xChange = GetSourceXoffset();
  yChange = GetSourceYoffset();

  //Mylar Disk
  MDOuterRadius = 2.38*cm/2;
  MDHalfHeight = 0.0254*cm/2;
  MDOffset = MDHalfHeight +GetSourceZoffset();

  //Kapton Disk
  KaptonOuterRadius = 2.38*cm/2;
  KaptonHalfHeight = .071*mm/2;
  KaptonOffset = -KaptonHalfHeight +GetSourceZoffset();

  //Copper Disk 1
```

```
  CD1OuterRadius = 2.38*cm/2;
  CD1HalfHeight = 0.1588*cm/2;
  CD1Offset = CD1HalfHeight +MDHalfHeight*2 +GetSourceZoffset();

  //Copper Disk 2
  CD2OuterRadius = 2.54*cm/2;
  CD2HalfHeight = 0.1588*cm/2;
  CD2Offset = -CD2HalfHeight -KaptonHalfHeight*2 -GetSourceZoffset();

  //Aluminum Ring
  AlInnerRadius = 2.38*cm/2;
  AlOuterRadius = 2.54*cm/2;
  AlHalfHeight = 0.318*cm/2;
  AlOffset = AlHalfHeight -MDHalfHeight*2 -KaptonHalfHeight*2;

 ;}

G4VPhysicalVolume* LTAC1DetectorConstruction::Construct()
{

 //===============BEGIN=Copper Disk 1=======================//

   G4Tubs *CDisk1 = new G4Tubs("Copper Disk 1", 0.0, CD1OuterRadius,
CD1HalfHeight, 0.0, 360.*deg);
   CDisk1_log = new G4LogicalVolume(CDisk1, Copper, "CDisk1_log", 0, 0, 0);
   CDisk1_phys = new G4PVPlacement(0, G4ThreeVector(xChange, yChange,
CD1Offset), CDisk1_log, "Copper Disk 1", Room_log, false, 0);
   G4VisAttributes CDisk1_Att(G4Color::Yellow());
   CDisk1_Att.SetForceWireframe(false);
   CDisk1_Att.SetForceSolid(true);
   CDisk1_Att.SetVisibility(true);
   CDisk1_log -> SetVisAttributes (CDisk1_Att);

 //===============END===Copper Disk 1=======================//

 //===============BEGIN=Copper Disk 2=======================//

   G4Tubs *CDisk2 = new G4Tubs("Copper Disk 2", 0.0, CD2OuterRadius,
CD2HalfHeight, 0.0, 360.*deg);
   CDisk2_log = new G4LogicalVolume(CDisk2, Copper, "CDisk2_log", 0, 0, 0);
   CDisk2_phys = new G4PVPlacement(0, G4ThreeVector(xChange, yChange,
CD2Offset), CDisk2_log, "Copper Disk 2", Room_log, false, 0);
   G4VisAttributes CDisk2_Att(G4Color::Yellow());
   CDisk2_Att.SetForceWireframe(false);
   CDisk2_Att.SetForceSolid(true);
   CDisk2_Att.SetVisibility(true);
   CDisk2_log -> SetVisAttributes (CDisk2_Att);

 //===============END===Copper Disk 2=======================//

 //===============BEGIN=Aluminum Ring=======================//
```

```
   G4Tubs *Ring = new G4Tubs("Ring", AlInnerRadius, AlOuterRadius,
AlHalfHeight, 0.0, 360.*deg);
   Ring_log = new G4LogicalVolume(Ring, Al, "Ring_log", 0, 0, 0);
   Ring_phys = new G4PVPlacement(0, G4ThreeVector(xChange, yChange, AlOffset),
Ring_log, "Ring", Room_log, false, 0);
   G4VisAttributes Ring_Att(G4Color::Gray());
   Ring_Att.SetForceWireframe(false);
   Ring_Att.SetForceSolid(true);
   Ring_Att.SetVisibility(true);
   Ring_log -> SetVisAttributes (Ring_Att);

 //===============END===Aluminum Ring=======================//*/

 //===============BEGIN=Mylar Disk=======================//

   G4Tubs *MylarDisk = new G4Tubs("Mylar Disk", 0.0, MDOuterRadius,
MDHalfHeight, 0.0, 360.*deg);
   MDisk_log = new G4LogicalVolume(MylarDisk, Mylar, "MDisk_log", 0, 0, 0);
   MDisk_phys = new G4PVPlacement(0, G4ThreeVector(xChange, yChange, MDOffset),
MDisk_log, "Mylar Disk", Room_log, false, 0);
   G4VisAttributes MDisk_Att(G4Color::Blue());
   MDisk_Att.SetForceWireframe(false);
   MDisk_Att.SetForceSolid(true);
   MDisk_Att.SetVisibility(true);
   MDisk_log -> SetVisAttributes (MDisk_Att);

 //===============END===Mylar Disk=======================//

 //===============BEGIN=Kapton Disk=======================//

   G4Tubs *KaptonDisk = new G4Tubs("Kapton Disk", 0.0, KaptonOuterRadius,
KaptonHalfHeight, 0.0, 360.*deg);
   KDisk_log = new G4LogicalVolume(KaptonDisk, Kapton, "KDisk_log", 0, 0, 0);
   KDisk_phys = new G4PVPlacement(0, G4ThreeVector(xChange, yChange,
KaptonOffset), KDisk_log, "Kapton Disk", Room_log, false, 0);
   G4VisAttributes KDisk_Att(G4Color::Green());
   KDisk_Att.SetForceWireframe(false);
   KDisk_Att.SetForceSolid(true);
   KDisk_Att.SetVisibility(true);
   KDisk_log -> SetVisAttributes (KDisk_Att);

 //===============END===Kapton Disk=======================//

}
```

A.2.2 Construction of Graphite Disks in "LTAC1DetectorConstruction.cc"

```
  //===============BEGIN=First Graphite Disk=======================//

  G4Tubs *Disk1 = new G4Tubs("Disk1", 0.0, C1OuterRadius, C1HalfHeight, 0.0,
360.*deg);
  Disk1_log = new G4LogicalVolume(Disk1, Graphite, "Disk1_log", 0, 0, 0);
  Disk1_phys = new G4PVPlacement(0, G4ThreeVector(0.0, 0.0, C1Zoffset),
Disk1_log, "Disk1", Room_log, false, 0);
  G4VisAttributes Disk1_Att(G4Color::Yellow());
  Disk1_Att.SetForceWireframe(false);
  Disk1_Att.SetForceSolid(true);
  Disk1_Att.SetVisibility(true);
  Disk1_log -> SetVisAttributes (Disk1_Att);

  //===============END===First Graphite Disk=======================//

  //===============BEGIN=Second Graphite Disk=======================//

   G4Tubs *Disk2 = new G4Tubs("Disk2", 0.0, C2OuterRadius, C2HalfHeight, 0.0,
360.*deg);
   Disk2_log = new G4LogicalVolume(Disk2, Graphite, "Disk2_log", 0, 0, 0);
   Disk2_phys = new G4PVPlacement(0, G4ThreeVector(0.0, 0.0, C2Zoffset),
Disk2_log, "Disk2", Room_log, false, 0);
   G4VisAttributes Disk2_Att(G4Color::Yellow());
   Disk2_Att.SetForceWireframe(false);
   Disk2_Att.SetForceSolid(true);
   Disk2_Att.SetVisibility(true);
   Disk2_log -> SetVisAttributes (Disk2_Att);

  //===============END===Second Graphite Disk=======================//
```

A.2.3 Construction of NaI detectors in "LTAC1DetectorConstruction.cc"

This code creates two identical NaI detectors whose positions are symmetric across the xy-plane. The NaI detectors are each composed of a NaI crystal, a BaO reflector on the face of the detector close to the source, and an aluminum shell that fully surrounds the detector.

```
//---------------BEGIN--- Geneseo NaI ----------------------//

// BEGIN NaI Crystal

  inner_radius = 0.0;
  outer_radius = NaI_radius;
  half_height = NaI_half_height;

  G4Tubs* NaI1 = new G4Tubs("NaI1", inner_radius, outer_radius,
```

```
     half_height, 0.0, 360.*deg);
  G4Tubs* NaI2 = new G4Tubs("NaI2",inner_radius, outer_radius,
     half_height, 0.0, 360.*deg);

  NaI1_log = new G4LogicalVolume(NaI1, NaI_Tl, "NaI1_log",0,0,0);
  NaI2_log = new G4LogicalVolume(NaI2, NaI_Tl, "NaI2_log",0,0,0);

  x_pos = 0.0*m;
  y_pos = 0.0*m;
  z_pos = NaI_half_height +gap/2.0 +NaIWallThickness +NaIReflectorThickness;

  // Place NaI 1 in room
  NaI1_phys = new G4PVPlacement(0,
     G4ThreeVector(x_pos, y_pos, z_pos),
     NaI1_log, "NaI1", Room_log, false, 0);

  z_pos = 0-z_pos;

  // Place NaI 2 in room
  NaI2_phys = new G4PVPlacement(0,
     G4ThreeVector(x_pos, y_pos, z_pos),
     NaI2_log, "NaI2", Room_log, false, 0);

  // END NaI Crystal

  // BEGIN REFLECTOR

  inner_radius = 0.0;
  outer_radius = NaI_radius +NaIReflectorThickness;
  half_height = NaI_half_height +NaIReflectorThickness;

  G4Tubs* RefSolid = new G4Tubs("RefSolid", inner_radius, outer_radius,
half_height, 0.0, 360.*deg);

  outer_radius = NaI_radius;
  half_height = NaI_half_height;
  G4Tubs* RefOut = new G4Tubs("RefOut", inner_radius, outer_radius,
half_height, 0.0, 360.*deg);

  Translation = new G4ThreeVector(0,0,0);
  Rotation = new G4RotationMatrix(0.,0.,0.);
  G4VSolid * reflectorShell = new G4SubtractionSolid("reflectorShell",
RefSolid, RefOut, Rotation, *Translation);

  NaI1Reflector_log = new
G4LogicalVolume(reflectorShell,BaO,"reflectorShell_log",0,0,0);
  NaI2Reflector_log = new
G4LogicalVolume(reflectorShell,BaO,"reflectorShell_log",0,0,0);

  x_pos = 0.0*m;
  y_pos = 0.0*m;
```

```
  z_pos = NaI_half_height +gap/2.0 +NaIReflectorThickness +NaIWallThickness;

  NaI1Reflector_phys = new G4PVPlacement(0, G4ThreeVector(x_pos, y_pos, z_pos),

NaI1Reflector_log,"NaI1Reflector",Room_log,false,0);

  z_pos = 0-z_pos;
  NaI2Reflector_phys = new G4PVPlacement(0, G4ThreeVector(x_pos, y_pos, z_pos),
     NaI2Reflector_log,"NaI2Reflector",Room_log,false,0);

  //Set attributes for visualization.
  G4VisAttributes NaIReflector_Att(G4Color::Red());
  NaIReflector_Att.SetVisibility(true);
  NaIReflector_Att.SetForceWireframe(true);
  NaIReflector_Att.SetForceAuxEdgeVisible(true);
  NaIReflector_Att.SetForceSolid(true);
  NaI1Reflector_log->SetVisAttributes (NaIReflector_Att);
  NaI2Reflector_log->SetVisAttributes (NaIReflector_Att);

// END REFLECTOR

  // BEGIN AL HOUSING
  inner_radius = 0.0;
  outer_radius = NaI_radius +NaIWallThickness +2.54*mm;
  half_height = NaI_half_height +NaIWallThickness;
  G4Tubs* alSolid = new G4Tubs("alSolid", inner_radius, outer_radius,
     half_height, 0.0, 360.*deg);
  outer_radius = NaI_radius;
  half_height = NaI_half_height;
  G4Tubs* cutOut = new G4Tubs("cutOut", inner_radius, outer_radius,
     half_height, 0.0, 360.*deg);

  Translation = new G4ThreeVector(0,0,0);
  Rotation = new G4RotationMatrix(0.,0.,0.);
  G4VSolid * aluminumShell = new G4SubtractionSolid("aluminumShell", alSolid,
     cutOut, Rotation, *Translation);
  // ALUMINUM SIDE WALLS

  NaI1Wall_log = new G4LogicalVolume(aluminumShell, Al, "alumimumShell_log", 0,
0, 0);
  NaI2Wall_log = new
G4LogicalVolume(aluminumShell,Al,"alumimumShell_log",0,0,0);

  x_pos = 0.0*m;
  y_pos = 0.*m;
  z_pos = NaI_half_height + gap/2.0 +NaIWallThickness +NaIReflectorThickness;
// For NaI cylinders and Al side wall cylinders

  NaI1Wall_phys = new G4PVPlacement(0, G4ThreeVector(x_pos, y_pos, z_pos),
                                    NaI1Wall_log, "NaI1Wall", Room_log, false,
0);
```

```
 z_pos = 0-z_pos;
 NaI2Wall_phys = new G4PVPlacement(0, G4ThreeVector(x_pos, y_pos, z_pos),
                     NaI2Wall_log,"Na2Wall",Room_log,false,0);

  G4VisAttributes NaI1_Att(G4Color::Blue());
  NaI1_Att.SetForceWireframe(true);
  NaI1_Att.SetForceSolid(true);
  NaI1_Att.SetForceAuxEdgeVisible(true);
  NaI1_Att.SetVisibility(true);
  NaI1_log -> SetVisAttributes (NaI1_Att);
  NaI2_log -> SetVisAttributes (NaI1_Att);

  G4VisAttributes NaIWall_Att(G4Color::Red());
  NaIWall_Att.SetVisibility(true);
  NaIWall_Att.SetForceWireframe(true);
  NaIWall_Att.SetForceAuxEdgeVisible(true);
  NaIWall_Att.SetForceSolid(true);
  NaI1Wall_log->SetVisAttributes (NaIWall_Att);
  NaI2Wall_log->SetVisAttributes (NaIWall_Att);

  inner_radius = NaI_radius;
  outer_radius = NaI_radius +NaIWallThickness;
  half_height = NaI_half_height +NaIWallThickness;


//---------------END--- GENESEO NaI ----------------------//
```

A.3 GEANT Monte-Carlo Sources

A.3.1 Positrons with ^{22}Na Energy Spread

Because the "Veto" detector used in Experiment IV eliminated the effects of 1275 keV gamma rays summing with 511 keV gamma rays, the GEANT simulation had to eliminate the effects of these gamma rays as well. Rather than simulate a source of ^{22}Na and the "Veto" detector in the GEANT code, only the positrons emitted by the ^{22}Na were simulated by assigning kinetic energies to simulated positrons that corresponded to those of positrons emitted by ^{22}Na. This eliminated the de-excitation 1275 keV gamma rays just as they were eliminated in the experimental measurement.

```
//------------------------------------------------------------------------
// INIT POSITION RAND POINT IN SOURCE CYL AS DEF IN LTAC1DetectorConstruction
//------------------------------------------------------------------------


//===== Set which side of the scintillator the particle is emitted from =====
```

```
  G4double source_side;
  G4int select_side = rand() % 2; //Creates a random number, 0 or 1.
  G4double source_half_height = myDetector->GetSourceHalfHeight();
  //Pull in the instance of the half_height of the source.

  // Uses random number to select which side the particle is released from,
  // slightly within scintillation source.
  if(select_side == 0) {source_side = -source_half_height;}
  else {source_side = source_half_height;}

  G4double zvalue = myDetector->GetSourceZoffset() + source_side;
  G4double rmin = myDetector->GetSourceInnerRadius();
  G4double rmax = myDetector->GetSourceRadius();
  G4double xmid = myDetector->GetSourceXoffset();
  G4double ymid = myDetector->GetSourceYoffset();

   //==== Side of emission has been set ======================
   //==== Setting Positron Energy with Spread ================

/* The energy spread for emitted positrons peaks at 178 keV and drops off
toward 0 keV and 540 keV in an almost linear slope. Here, I am simulating that
slope as a line. There is a function for the rising slope and the falling slope
   rising:  energy = 178keV *(random y value from 0 to 1)
   falling: energy = 362keV *[(random y value from 0 to 1) -1.491727]
A random number called halfSelect (0 or 1) selects which function is used to
set the energy. */

  G4int halfSelect = rand() %2;
  G4double energySelect = ((G4double)rand()/(G4double)RAND_MAX);
  G4double pEnergy;

  if( halfSelect = 1 ){ pEnergy = 178.0 *energySelect; }
       else { pEnergy = -362.0 *(energySelect -1.491727); }

  //==== Positron energy has been set ==========================

  G4double zStart = zvalue; // z from source_side
  G4double phiStart = G4RandFlat::shoot(0.,2.*3.1415926); // random phi
  G4double rStart = sqrt(G4RandFlat::shoot(pow(rmin,2.),pow(rmax,2.)));
  // random r^2 value
  G4double xStart = xmid + rStart*cos(phiStart);
  G4double yStart = ymid + rStart*sin(phiStart); // y value using random phi
  particleGun->SetParticleEnergy(pEnergy*keV);

  // RANDOM DIRECTION, FROM EXAMPLE. CAREFUL WITH NORMALIZATION.
  G4double a,b,c;

  G4double n;
  do {
   a=(G4UniformRand()-0.5)/.5;
   b=(G4UniformRand()-0.5)/.5;
```

```
   c=(G4UniformRand()-0.5)/.5;
  n = a*a+b*b+c*c;
  } while (n > 1 || n == 0.0);
  n = std::sqrt(n);
  a /= n;
  b /= n;
  c /= n;

  if(select_side == 0) {c =  abs(c);}
     else {c = -abs(c);}

  G4ThreeVector direction(a,b,c);
  particleGun->SetParticleMomentumDirection(direction);
  particleGun->SetParticlePosition(G4ThreeVector(xStart,yStart,zStart));
  particleGun->GeneratePrimaryVertex(anEvent); // create vertex
}
```

A.3.2 The ^{68}Ga Source

```
//--------------------------------------------------------------------------
// INIT POSITION RAND POINT IN SOURCE CYL AS DEF IN LTAC1DetectorConstruction
//--------------------------------------------------------------------------

  //==== Set which side of the source the particle is emitted from ========
  G4double source_side;
  G4int select_side = rand() % 2; //Creates a random number, 0 or 1.
  G4double source_half_height = myDetector->GetSourceHalfHeight();

  if(select_side == 0) {source_side = -source_half_height;}
  else {source_side = source_half_height;}

  G4double rmax = 0.3*cm;//myDetector->GetSourceRadius();
  G4double xmid = myDetector->GetSourceXoffset();
  G4double ymid = myDetector->GetSourceYoffset();

  //==== Side of emission has been set ======================================

  G4double zStart = 0.0*cm;//G4RandFlat::shoot(zmin, zmax);
  G4double phiStart = G4RandFlat::shoot(0.,2.*3.1415926); // random phi
  G4double rStart = sqrt(G4RandFlat::shoot(pow(rmin,2.),pow(rmax,2.)));
  // random r^2 value
  G4double xStart = xmid + rStart*cos(phiStart);
  G4double yStart = ymid + rStart*sin(phiStart);
  // y value using random phi
  particleGun->SetParticleEnergy(0.0*keV);

  // RANDOM DIRECTION, FROM EXAMPLE. CAREFUL WITH NORMALIZATION.
```

```
  G4double a,b,c;

  G4double n;
  do {
   a=(G4UniformRand()-0.5)/.5;
   b=(G4UniformRand()-0.5)/.5;
   c=(G4UniformRand()-0.5)/.5;
  n = a*a+b*b+c*c;
  } while (n > 1 || n == 0.0);
  n = std::sqrt(n);
  a /= n;
  b /= n;
  c /= n;

  if(select_side == 0) {c =  abs(c);}
     else {c = -abs(c);}

  G4ThreeVector direction(a,b,c);
  particleGun->SetParticleMomentumDirection(direction);
  particleGun->SetParticlePosition(G4ThreeVector(xStart,yStart,zStart));
  particleGun->GeneratePrimaryVertex(anEvent); // create vertex
}
```

References

[1] F. Winterberg, *The Release of Thermonuclear Energy by Inertial Confinement*, (World Scientific, 2010) p. 9
[2] LLE Review **69**, 46 (1996).
[3] "Q-Value Calculator" [Online]. National Nuclear Data Center. http://www.nndc.bnl.gov/qcalc
[4] D. R. Welch, H. Kislev, and G. H. Miley, Rev. Sci. Instrum. **59**, 610 (1988).
[5] G. Hartshaw, *A Measurement of the $^{12}C(n, 2n)^{11}C$ Cross Section for use as an Inertial Confinement Fusion Diagnostic,* Thesis, Houghton College, 2014.
[6] J. E. Brolley Jr., J. L. Fowler, and L. K. Schlacks, Phys. Rev. **88**, 618 (1952)
[7] O. D. Brill, N. A. Vlasov, S. P. Kalnin, and L. S. Sokolov, Sov. Phys. Doklady **6**, 24 (1961).
[8] B. Anders, P. Herges, and W. Scobel, Z. Phys. A **301**, 353 (1981).
[9] P. Welch, J. Johnson, G. Randers-Pehrson, and J. Rapaport, Data file EXFOR-12912.004, compare Bull. Am. Phys. Soc. **26**, 708 (1981).
[10] T. S. Soewarsono, Y. Uwamino, and T. Nakamura, JAERI Tokai Rep. **27**, 354 (1992).
[11] Y. Uno, Y. Uwamino, T. S. Soewarsono, and T. Nakamura, Nucl. Sci. Eng. **122**, 27 (1996).
[12] P. J. Dimbylow, Phys. Med. Biol. **25**, 637 (1980).
[13] "Chart of Nuclides" [Online]. National Nuclear Data Center. http://www.nndc.bnl.gov/chart
[14] V. Stoks, R. Klomp, M. Rentmeester, and J. De Swart, Phys. Rev. C **48**, 792 (1993).
[15] V. Stoks, R. Klomp, C. Terheggen, and J. De Swart, Phys. Rev. C **49**, 2950 (1994).
[16] M. Drosg, Tech. Rep. IAEA-NDS-87 Rev. 9, International Atomic Energy Agency, Nuclear Data Section, Vienna (Austria) (2005).
[17] N. Tsoulfanidis, *Measurement and Detection of Radiation* 2nd ed., (Taylor & Francis, 1995) p. 286, 394.
[18] S. Yalcin, O. Gurler, G. Kaynak, and O. Gundogdu, Appl. Rad. and Isotopes **65**, 1179 (2007).
[19] ORTEC, 905 Series NaI(Tl) Scintillation Detectors (2016).
[20] J. Streets and D. Slimmer, *LINUX IEEE CAMAC Library for the Jorway 411S SCSI CAMAC Driver and the Jorway 73A SCSI CAMAC Crate Controller*, (Fermilab, 2002).
[21] Rene Brun and Fons Rademakers, ROOT - An Object Oriented Data Analysis Framework, Proceedings AIHENP '96 Workshop, Lausanne, Sep. 1996, Nucl. Inst. & Meth. in Phys. Res. A **389** (1997) 81-86. See also http://root.cern.ch/.
[22] E. Schöenfeld, U. Schoetzig, E. Guenther, and H. Schrader, Appl. Rad. and Isotopes, **45**, 955 (1994).